HHS Public Access

Author manuscript

New Phytol. Author manuscript; available in PMC 2025 January 01.

Published in final edited form as:

New Phytol. 2024 January ; 241(2): 687–702. doi:10.1111/nph.19383.

Phosphoproteome analyses pinpoint the F-box protein SLOW MOTION as a regulator of warm temperature-mediated hypocotyl growth in *Arabidopsis*

Shanshuo Zhu[1,2,3,4,*], **Lixia Pan**[1,2,*], **Lam Dai Vu**[1,2,3,4,*], **Xiangyu Xu**[1,2], **Beatriz Orosa-Puente**[5,6], **Tingting Zhu**[1,2], **Pia Neyt**[1], **Brigitte van de Cotte**[1,2], **Thomas B. Jacobs**[1,2], **Joshua M. Gendron**[7], **Steven H. Spoel**[5], **Kris Gevaert**[3,4,†], **Ive De Smet**[1,2,†]

[1]Department of Plant Biotechnology and Bioinformatics, Ghent University, B-9052, Ghent, Belgium;

[2]VIB Center for Plant Systems Biology, B-9052, Ghent, Belgium;

[3]VIB-UGent Center for Medical Biotechnology, VIB, B-9000, Ghent, Belgium;

[4]Department of Biomolecular Medicine, Ghent University, B-9000, Ghent, Belgium;

[5]Institute of Molecular Plant Sciences, School of Biological Sciences, University of Edinburgh, Edinburgh, EH9 3BF, UK;

[6]Centro Singular de Investigación en Química Biolóxica e Materiais Moleculares (CIQUS) and Departamento de Química Orgánica, Universidade de Santiago de Compostela, 15782, Santiago de Compostela, Spain;

[7]Department of Molecular, Cellular, and Developmental Biology, Yale University, New Haven, CT 06511, USA

Summary

- Hypocotyl elongation is controlled by several signals and is a major characteristic of plants growing in darkness or under warm temperature. While already several molecular mechanisms associated with this process are known, protein degradation and associated E3 ligases have hardly been studied in the context of warm temperature.

Author for correspondence: *Ive De Smet*, ive.desmet@psb.vib-ugent.be.
*These authors contributed equally to this work.
†These authors jointly supervised this work.

Author contributions

SZ, IDS, TBJ, SHS, LDV, LP and KG designed research; SZ, LP, XX, TZ, BC, PN, BO-P and LDV performed the experiments and/or analysed data; JMG provided reagents and/or expertise; IDS, SHS and KG analysed data; and SZ, LP, LDV, KG and IDS wrote the paper. All authors contributed to the writing of the paper. SZ, LP and LDV contributed equally to this work. IDS and KG jointly supervised this work.

Competing interests

None declared.

Supporting Information

Additional Supporting Information may be found online in the Supporting Information section at the end of the article.
Please note: Wiley is not responsible for the content or functionality of any Supporting Information supplied by the authors. Any queries (other than missing material) should be directed to the *New Phytologist* Central Office.

- In a time-course phosphoproteome analysis on *Arabidopsis* seedlings exposed to control or warm ambient temperature, we observed reduced levels of diverse proteins over time, which could be due to transcription, translation, and/or degradation. In addition, we observed differential phosphorylation of the LRR F-box protein SLOMO MOTION (SLOMO) at two serine residues.
- We demonstrate that SLOMO is a negative regulator of hypocotyl growth, also under warm temperature conditions, and protein–protein interaction studies revealed possible interactors of SLOMO, such as MKK5, DWF1, and NCED4. We identified DWF1 as a likely SLOMO substrate and a regulator of warm temperature-mediated hypocotyl growth.
- We propose that warm temperature-mediated regulation of SLOMO activity controls the abundance of hypocotyl growth regulators, such as DWF1, through ubiquitin-mediated degradation.

Keywords

DWARF1; hypocotyl; (phospho) proteomics; SLOW MOTION; thermomorphogenesis

Introduction

Hypocotyl elongation is controlled by environmental as well as developmental signals and affected by hormones, light, and the circadian clock (Quint *et al.*, 2016; Jin & Zhu, 2019) and is a major characteristic of plants growing in darkness or under warm temperature (Josse & Halliday, 2008; Casal & Balasubramanian, 2019). Warm temperature-mediated growth regulation through chromatin remodeling (Tasset *et al.*, 2018; Xue *et al.*, 2021), plant hormone-mediated signaling (Castroverde & Dina, 2021; Li *et al.*, 2021; Zhu *et al.*, 2021), transcriptional regulators (Leivar & Monte, 2014; Ohama *et al.*, 2016; Quint *et al.*, 2016; Qiu *et al.*, 2019), and mRNA translation (Chung *et al.*, 2020) is well understood. In addition to these mechanisms, less-explored protein phosphorylation-driven signaling (Praat *et al.*, 2021; Vu *et al.*, 2021) and ubiquitin-mediated protein degradation (Chiu *et al.*, 2016; Liu *et al.*, 2020) also play roles during thermomorphogenesis. In general, protein ubiquitination is achieved via sequential action of E1, E2 and E3 enzymes to attach evolutionarily-conserved ubiquitin (Ub) to target proteins, with E3 ligases determining the substrate specificity (Hershko & Ciechanover, 1998). The structures and mechanisms of these E3 ligases are diverse (Chen & Hellmann, 2013). Plant E3 ligases can be divided into monomeric and multimeric E3 ligases. Depending on the mechanism by which ubiquitin is transferred from the E2 enzyme to the substrate, monomeric E3 ligases are classified into Really Interesting New Gene (RING) finger domain-, homologous to E6-associated protein C terminus (HECT) domain-, or RING Between RING (RBR) domain-containing ubiquitin ligases (Balaji & Hoppe, 2020). In addition, multimeric E3 ligase complexes contain a CULLIN protein that serves as the scaffold for the binding of a RING-BOX1, which recruits an E2 ligase and a substrate-binding subunit. In the case of the SKP1-CULLIN-F-box (SCF) complex, the substrate-binding F-box protein is tethered to the CUL1 (CULLIN 1) scaffold by SKP1; while for the CULLN4-RING ligase (CRL4) complex,

CUL4 uses DNA damage binding protein 1 (DDB1) as adaptor and CUL4-associated factors (DCAFs) as substrate receptors to identify a large number of substrate proteins (Bulatov & Ciulli, 2015). Altogether, there are over 1500 predicted E3 ligases in *Arabidopsis* (Chen & Hellmann, 2013), yet despite this large number only a few have been studied in the context of high temperature. For example, the E3 ubiquitin ligase CONSTITUTIVE PHOTOMORPHOGENIC 1 (COP1) and its target ELONGATED HYPOCOTYL 5 (HY5) could convey warm temperature signals to hypocotyl thermomorphogenesis (Delker *et al.*, 2014; Gangappa & Kumar, 2017; Park *et al.*, 2017; B. Zhang *et al.*, 2017). In addition, the E3 ligase PLANT U-BOX 48 (PUB48) plays pivotal roles during seed germination and plant growth under heat stress (Peng *et al.*, 2019), while the E3 ligase XB3 ORTHOLOG 1 IN ARABIDOPSIS THALIANA (XBAT31) regulates thermoresponsive hypocotyl growth via mediating the degradation of the thermosensor EARLY FLOWERING3 (ELF3; Zhang *et al.*, 2021b). Finally, CULLIN3 BLADE-ON-PETIOLE1 (BOP1) and BOP2 E3 ligases regulate hypocotyl thermomorphogenesis via modulating PHYTOCHROME-INTERACTING FACTOR 4 (PIF4) ubiquitination (Morimoto *et al.*, 2017; Liu *et al.*, 2020).

Here, in a time-course (phospho)proteome analysis on *Arabidopsis* seedlings exposed to control or high ambient temperature, we observed reduced levels of > 200 proteins over time, which could be in part due to changes in gene transcription, mRNA translation, and/or protein degradation. In addition, we observed differential phosphorylation of the LRR F-box protein SLOMO MOTION (SLOMO) at two serine residues. We demonstrated that SLOMO is a negative regulator of hypocotyl growth, and protein–protein interaction studies revealed possible interactors of SLOMO. We identified DWF1 as a likely SLOMO substrate and a regulator of warm temperature-mediated hypocotyl growth. In conclusion, our results show that regulation of protein levels, and specifically SLOMO-mediated regulation of protein levels, plays an important role in (warm temperature-mediated) hypocotyl growth.

Materials and Methods

Plant materials and growth conditions

The following *Arabidopsis thaliana* (L.) Heynh. lines were used: *slomo-3* (*SALK_091125*) (Lohmann *et al.*, 2010), *pSLOMO:: GUS* (Lohmann *et al.*, 2010), *slomo-4* (*SALK_013287*), *dwf1* (*SALK 006932*) (Youn *et al.*, 2018), *ccd4–2* (*SALK_097984*) (Rottet *et al.*, 2016), *mkk5–18* (Till *et al.*, 2003), *phot1–5* (Kinoshita *et al.*, 2001), and *35S::DWF1:YFP* (Silvestro *et al.*, 2013). *pSLOMO::GUS* is in the Landsberg *erecta* background, the tilling line *mkk5–18* is in the Col *er-105* background, and the other lines are in a Col-0 background. Seeds were gas sterilized, sown on horizontal plates, vernalized at 4°C for 48 h, and then transferred to 21°C for germination for 48 h. Plates were then transferred to short-day conditions (8 h : 16 h, light : dark; 100 μmol m^{-2} s^{-1} photosynthetically active radiation, supplied by cool-white, fluorescent tungsten tubes, Osram; and 65–75% air humidity). For (phospho)proteome analyses, plants were grown at 21°C for 7 d and at the beginning of the seventh night, one half of the plants was transferred to 28°C while the other half was kept at 21°C. Samples of plants kept at both temperatures were harvested at 15, 30, 120, and 960 min in four independent replicates. For phenotypic characterization, plants were grown at short-day conditions for 7 d, unless otherwise indicated.

Protein extraction and phosphopeptide enrichment

Protein extraction and phosphopeptide enrichment were performed according to our previously described procedure (Vu *et al.*, 2018b). In brief, 1 g of finely ground plant material was suspended in homogenization buffer containing 30% sucrose, 250 mM Tris–HCl buffer (pH 8), 5 mM EDTA, and 500 mM dithiothreitol (DTT) in Milli-Q water, to which the appropriate amounts of the cOmplete™ protease inhibitor mixture (Roche) and the PhosSTOP phosphatase inhibitor mixture (Roche) were added. The samples were sonicated on ice and centrifuged at 4°C for 15 min at 2500 ***g*** to remove debris. Supernatants were collected, and a methanol/chloroform precipitation was carried out by adding 3, 1, and 4 volumes of methanol, chloroform and water, respectively. Samples were centrifuged for 10 min at 5000 ***g***, and the aqueous phase was removed. After the addition of four volumes of methanol, the proteins were pelleted via centrifugation for 10 min at 2500 ***g***. Pellets were washed with 80% acetone and centrifuged for 10 min at room temperature at 2500 ***g***. The supernatants were discarded, and the pellets were let to dry on air. Protein pellets were then resuspended in 8 M urea in 50 mM triethylammonium bicarbonate (TEAB) buffer (pH 8). Alkylation of cysteines was carried out by adding tris(carboxyethyl)phosphine (TCEP; Pierce, Rockford, lL, USA) and iodoacetamide (Sigma-Aldrich) to final concentrations of 15 and 30 mM, respectively, and the samples were incubated for 15 min at 30°C in the dark. Next, 5 mg of protein material was predigested with MS-grade lysyl endopeptidase (Wako Chemicals, Osaka, Japan) for 4 h at 37°C at an enzyme : substrate ratio of 1 : 500 (w/w). The mixtures were diluted eightfold with 50 mM TEAB, followed by an overnight digestion with trypsin (Promega) with an enzyme : substrate ratio of 1 : 100 (w/w). The digest was acidified to pH 3 with trifluoroacetic acid (TFA) and desalted using SampliQ C18 SPE cartridges (Agilent, Santa Clara, CA, USA) according to the manufacturer's guidelines. The desalted peptides were fully dried in a vacuum centrifuge and then resuspended in 500 µl of loading solvent (80% (v/v) acetonitrile, 5% (v/v) TFA). Finally, 100 µl of the resuspended peptides was vacuum-dried and retained for proteome analysis. For phosphopeptide enrichment, 400 µl of the resuspended peptides was incubated with 1 mg MagReSyn® Ti-IMAC microspheres for 20 min at room temperature with continuous mixing. The microspheres were washed once with wash solvent 1 (60% acetonitrile, 1% TFA, 200 mM NaCl) and twice with wash solvent 2 (60% acetonitrile, 1% TFA). The bound phosphopeptides were eluted with three volumes (80 µl) of elution buffer (40% acetonitrile, 5% NH_4OH), immediately followed by acidification to pH 3 using formic acid. Before MS analysis, the samples were vacuum-dried and re-dissolved in 50 µl of 2% (v/v) acetonitrile and 0.1% (v/v) TFA.

LC–MS/MS analysis

For phosphoproteome and proteome analysis, four or three independent biological replicates were analyzed using LC–MS/MS, respectively. Each sample was analyzed via LC–MS/MS on an Ultimate 3000 RSLC nano-LC (Thermo Fisher Scientific, Bremen, Germany) in-line connected to a Q Exactive mass spectrometer (Thermo Fisher Scientific). The peptides were first loaded on a trapping column (made in-house, 100 µm internal diameter (ID) × 20 mm, 5 µm beads C18 Reprosil-HD; Dr Maisch, Ammerbuch-Entringen, Germany). After flushing the trapping column, peptides were loaded in solvent A (0.1% formic acid

in water) on a reverse-phase column (made in-house, 75 μm ID × 250 mm, 1.9 μm Reprosil-Pur-basic-C18-HD beads; Dr Maisch, packed in the needle) and eluted by an increase in solvent B (0.1% formic acid in acetonitrile) using a linear gradient from 2% solvent B to 55% solvent B in 120 min, followed by a washing step with 99% solvent B, all at a constant flow rate of 300 nl min^{-1}. The mass spectrometer was operated in data-dependent, positive ionization mode, automatically switching between MS and MS/MS acquisition for the five most abundant peaks in a given MS spectrum. The source voltage was set at 4.1 kV and the capillary temperature at 275°C. One MS1 scan (*m/z* 400_2000, AGC target 3×10^6 ions, maximum ion injection time 80 ms), acquired at a resolution of 70 000 (at 200 *m/z*), was followed by five tandem MS scans (resolution 17 500 at 200 *m/z*) of the most intense ions fulfilling predefined selection criteria (AGC target 5×10^4 ions, maximum ion injection time 80 ms, isolation window 2 Da, fixed first mass 140 *m/z*, spectrum data type: centroid, under-fill ratio 2%, intensity threshold 1.3 × E4, exclusion of unassigned, 1, 5–8, > 8 positively charged precursors, peptide match preferred, exclude isotopes on, dynamic exclusion time 12 s). The HCD collision energy was set to 25% normalized collision energy, and the polydimethylcyclosiloxane background ion at 445.120025 Da was used for internal calibration (lock mass).

Database searching

MS/MS spectra were searched against the TAIR10 *Arabidopsis* protein sequence database (35 386 entries, v.14.12.2010) with the MaxQuant software (v.1.5.4.1). The precursor mass tolerance set to 20 ppm for the first search (used for nonlinear mass recalibration) and to 4.5 ppm for the main search. Trypsin was selected as enzyme setting. Cleavages between lysine/argininepro-line residues and up to two missed cleavages were allowed. *S*-carbamidomethylation of cysteine residues was selected as a fixed modification, and protein N-acetylation and oxidation of methionine residues were selected as a variable modification. For phosphoproteome analysis, phospho (STY) was added as the additional variable modification. The false discovery rate for peptide and protein identifications was set to 1%, and the minimum peptide length was set to 7. The minimum score threshold for both modified and unmodified peptides was set to 30. The MaxLFQ algorithm allowing for label-free quantification (Cox *et al.*, 2014) and the ‘matching between runs’ feature were enabled. For the calculation of protein ratios, both unique and razor peptides (nonunique peptides that are assigned to a protein group with the largest number of identified peptides) were selected. All MS proteomics data have been deposited to the ProteomeXchange Consortium via the PRIDE partner repository (Perez-Riverol *et al.*, 2019) with the dataset identifiers PXD035922 and PXD028319.

Statistical analysis

MaxQuant output results were prefiltered for sequences matched with contaminants or decoy reverse database. Proteins that were only identified by modification site were also discarded in the proteome dataset. For phosphoproteome analysis, only phosphosites with localization probability ≥ 0.75 were retained for further analysis. Each phosphosite/protein group was analyzed separately by fitting a linear mixed model of the following form:

$$y_{jkl} = \mu + \beta_j + \gamma_k + (\beta\gamma)_{jk} + \delta_l + \epsilon_{jkl}$$

where, y_{jkl} = the $\log_2$-transformed intensity measured in the l^{th} replicate (l = 1…4) at the j^{th} temperature (j = 1…2; 21°C and 28°C) at the k^{th} time point (k = 1…4; 15, 30, 120 and 960 min).

The fixed part of the model consists of μ, the overall constant (general mean); β_j, the main effect of the j^{th} temperature; γ_k, the main effect of the k^{th} time; and $(\beta\gamma)_{jk}$, their interaction.

The random model terms, assumed to follow a normal distribution with zero mean and variance σ^2, are δ_l, the effect of the replicate l; and ε_{jkl}, the random error (i.e. residual) for sample *jkl*.

To examine to what extent significant changes observed in phosphorylation abundances in response to temperature and time were independent from changes in protein level, phosphosite intensities and LFQ intensities quantities were analyzed jointly and the linear mixed model described above was extended as follows:

$$y_{ijkl} = \mu + \alpha_i + \beta_j + \gamma_k + (\alpha\beta)_{ij} + (\alpha\gamma)_{ik} + (\beta\gamma)_{jk} + (\alpha\beta\gamma)_{ijk} + \delta_l + \varepsilon_{ijkl}$$

where, y_{ijkl}, the $\log_2$-transformed LFQ intensity of the peptide or phosphopeptide quantity measured in sample *jkl*; α_i, is the additional main term modeling the phosphorylation effect; $(\alpha\beta)_{ij}$, $(\alpha\gamma)_{ik}$, $(\beta\gamma)_{jk}$ and $(\alpha\beta\gamma)_{ijk}$ are the additional interactions; and ε_{ijkl} the random error (i.e. residual) for sample *ijkl*.

Both linear mixed models were fitted by the residual maximum likelihood (REML) approach as implemented in GENSTAT v.19 (www.genstat.co.uk). Significances of the fixed main effects and their interactions were assessed by an *F*-test, and corresponding false discovery rates (FDR) were calculated by modelling the probabilities as a mixture distribution as implemented in GENSTAT v.19.

Hierarchical clustering

Log_2 phosphosite intensities were *Z*-scored before clustering. Hierarchical clustering was carried out in Perseus (1.5.5.3), using the default settings. Both rows and columns were selected for the clustering using Euclidean distance. Average linkage is used to calculate the inter-cluster distance. Data were preprocessed using *k*-means, with the number of clusters created by the *k*-means algorithm being set at 300.

In silico analyses

For the Gene Ontology (GO) analysis, GO enrichment analyses were performed using Dicots Plaza 4.5 workbench (Van Bel *et al.*, 2018). The significant proteins and phosphoproteins regulated by only temperature and by the interaction of time and temperature were enriched for GO categories by using the whole species as the background model. Significance settings were set at a *P*-value cutoff < 0.05, and Bonferroni correction for multiple testing was used. For the Venn diagrams, an online tool (https://

bioinfogp.cnb.csic.es/tools/venny/) was used. For the SLOMO protein sequence alignment, Clc Main Workbench 20.03 (CLC Bio-Qiagen, Aarhus, Denmark) was used.

Co-immunoprecipitation

For transient co-agroinfiltration of tobacco leaves, *Agrobacteria* containing the indicated constructs and P19 were grown in 5 ml LB supplemented with appropriate antibiotics at 28°C for 1–2 d. Then, 500 µl was inoculated in 10 ml LB supplemented with 10 mM MES pH 5.6, 10 µM acetosyringone as well as the antibiotics and grown at 28°C overnight. The pellet was spun down and resuspended with infiltration buffer (10 mM $MgCl_2$, 10 mM MES (pH 5.6), 100 µM acetosyringone) to a final OD_{600} of 1.0. Equal volumes of three agrobacteria with selected constructs were mixed well, and the mix was infiltrated in tobacco leaves using a syringe. The signal was checked by confocal microscopy after 72 h to make sure the protein expressed well. Total proteins were extracted with buffer containing 150 mM Tris–HCl, pH 7.5, 150 mM NaCl, 10% glycerol, 100 mM EDTA, 1 mM sodium molybdate, 1 mM NaF, 10 mM DTT, 1% NP-40, 1 mM PMSF, and EDTA-free protease inhibitor mixture complete (Roche). The protein concentration was measured using the Qubit™ Protein Assay Kit (Carlsbad, CA, USA), and an equal amount of total protein was used for immunoprecipitation. The 25 µl of pre-equilibrated GFP-Trap®_MA beads (ChromoTek, Planegg/Martinsried, Germany) was prewashed three times with 700 µl wash buffer (20 mM Tris–HCl, pH 7.5, 150 mM NaCl and 0.5% NP-40). The homogenates were incubated with GFP-Trap®_MA beads and rotated for 2 h at 4°C to maximize protein binding. Subsequently, the solution was removed and the beads were washed three times with wash buffer (20 mM Tris–HCl pH 7.5, 150 mM NaCl and 0.5% NP-40). Finally, 1× sample buffer (Bio-Rad) was added to elute protein from beads.

Immunoprecipitation-mass spectrometry analysis

Sample preparation was performed as reported previously (Vu *et al.*, 2021). LC–MS/MS analysis was performed as described previously (Vu *et al.*, 2016). The peptides were analyzed on an Ultimate 3000 RSLC nano-LC on-line connected to a Q Exactive mass spectrometer (ThermoFisher Scientific). MS/MS spectra were searched against GFP:SLOMO and GFP:SLOMO-Decoy protein sequences and the *Arabidopsis* proteome database (TAIR10, 34 509 entries, version November 2014; http://www.arabidopsis.org/). To detect the interactors of SLOMO following immunoprecipitation-mass spectrometry (IP-MS), MaxQuant software (v.1.5.4.1) was used with settings for MaxQuant searches as previously reported (Vu *et al.*, 2016). After MS-based identification of co-immunoprecipitated proteins, proteins were selected as putative interactors if they were present in at least three out of four experimental samples and totally absent in all control samples. For the detection of the phosphorylation sites following IP-MS, peptide searches were performed using the MaxQuant software (v.1.6.17.0) on the UseGalaxy.be server and phospho (STY) was added as the additional variable modification. The MaxLFQ algorithm allowing for label-free quantification and the ‘matching between runs’ feature were enabled.

Mass spectrometry analysis for DWF1 ubiquitination in tobacco leaves

Transient co-agroinfiltration of tobacco leaves, total protein extraction, and GFP:DWF1 immunoprecipitation were performed as described previously (see 'Co-immunoprecipitation' in the Materials and Methods section). Following the co-immunoprecipitation (co-IP), the sample preparation is the same as the sample preparation procedure described previously (see 'Immunoprecipitation-mass spectrometry analysis' in the Materials and Methods section), except that 750 mM chloroacetamide instead of iodoacetamide was used for protein alkylation. LC–MS/MS analyses were carried out as described previously (see 'Immunoprecipitation-mass spectrometry analysis' in the Materials and methods section). Peptide searches were performed using the MaxQuant software (v.1.6.17.0) on the UseGalaxy.be server. A database containing all *Nicotiana benthamiana* protein sequences from SolGenomics and the protein sequences of GFP: DWF1 and mCherry:SLOMO was used as the search database. Gly Gly (K) was added as the additional variable modification. The MaxLFQ algorithm allowing for label-free quantification and the 'matching between runs' feature were enabled.

Generation of constructs and transgenic lines

The iProof High-Fidelity polymerase (Bio-Rad) was used for PCR to amplify *SLOMO* genomic DNA (to generate *pSLOMO:: GFP:SLOMO* and *35S:mCherry:SLOMO*), *SLOMO* promoter (1741 base pairs upstream of *SLOMO*), and the coding sequence (CDS) of *DWF1*, *MKK5*, and *NCED4*. The *SLOMO-Decoy* was synthesized using the BioXP3200™ system (SGI-DNA, San Diego, CA, USA) with the *SLOMO* CDS sequence by removing sequences (190–236 bp) coding the F-BOX domain of the SLOMO protein. For the cloning, the genomic DNA, CDS, or the promoter of interest were cloned into the Gateway entry vector pDONR221 or pDONRP4-P1r and then recombined into the desired destination vector (Karimi *et al.*, 2002). Plant vectors were transformed in *Agrobacterium tumefaciens* C58C1 using a freeze–thaw method (Clough & Bent, 1998). Plant transformation was performed using floral dip method (Clough & Bent, 1998). All transgenic plants contain the Basta resistance marker. All primers are listed in Supporting Information Table S1.

Genome editing of SLOMO

To generate the *slomo-5* mutant, we used Golden Gate cloning to create the CRISPR-Cas9 vector following approach as described previously (Decaestecker *et al.*, 2019). Two gRNA primers were designed (Table S1), and PCR was performed by using *pEN-2xAtU6–26* as template. The PCR products were run on 1% agarose gel, and the 575 bp band was gel purified for following assembling into the destination vector *pGGB AtCas9* via a Golden Gate reaction. The vector was checked via Sanger sequencing to verify the inserted fragment. Selection PCRs were performed with SLOMO_F1_Fwd and SLOMO_F1_Rev primers (Table S1) on the genomic DNA of the transgenic plants. The PCR products were analysed via agarose gel electrophoresis, and the purified samples were sent for Sanger sequencing with the SLOMO_F1_Fwd primer (Table S1) and analysed using TIDE (Brinkman *et al.*, 2014). The Cas9-free homozygous *slomo-5* line with desired gene editing was obtained through sequence analysis at the T3 generation, and phenotyping was performed on the T4 generation.

Histochemical GUS assays

For GUS assays, seedlings were put overnight in 90% acetone and rinsed with NT buffer (100 mM Tris/50 mM NaCl), then transferred to a GUS-solution (500 µl 100 mM $K_3[Fe(CN)_6]$ + 600 µl X-Gluc + 28.8 ml NT buffer), and incubated at 37°C in the dark. The reaction was stopped by rinsing with NT buffer, and then, seedlings were mounted in 80% lactic acid on a slide and imaged.

Confocal microscopy

Seedlings were mounted in Milli-Q water between the slide and cover glass for imaging using a Zeiss inverted LSM710 confocal laser scanning microscope, equipped with a LD-Plan Neofluar ×40/0.6 Korr M27 or C-Apochromat ×40/1.20 W Korr M27. A 488 nm laser excitation (at 2% power) of a 20 mW argon laser (LASOS, Jena, Germany) and a spectral detection bandwidth of 493–532 or 493–579 nm were used for detecting eGFP. For pro-pidium iodide (PI) staining, whole seedlings were mounted in PI solution. The PI signal was detected using a 561 nm laser excitation (at 2% power), together with a spectral detection bandwidth of 596–645 nm.

qPCR analyses

Three or four biological replicates were performed for each condition. Total RNA was extracted with the RNeasy Mini Kit (Qiagen) according to the manufacturer's instructions. DNA digestion was done on columns with RNase-free DNase I (Promega). The iScript cDNA Synthesis Kit (Bio-Rad) was used for cDNA synthesis from 1 µg of RNA. qRT-PCR was performed on a LightCycler 480 (Roche Diagnostics) in 384-well plates with LightCycler 480 SYBR Green I Master (Roche) according to the manufacturer's instructions. Two housekeeping genes, the *ACTIN-RELATED PROTEIN 7* (*ARP7*) and the *TRANSLATIONAL ELONGATION FACTOR ALPHA* (*EF1*α), were used for normalization of the expression level of the tested genes. Data analysis was performed with the QBASE$^+$ software. All the primers are listed in Table S1.

Analyses of cellular ubiquitin conjugates

Halo-Ubiquilin protein (DU no.: DU39178; Genbank: NM_ 053067.2) was expressed in *Escherichia coli* at 24°C for 6 h after induction with 1 mM IPTG. Halo-Ubiquilin was then purified using Halo beads (Promega; binding capacity 20 mg ml^{-1}) as recommended by the manufacturer. *Arabidopsis* seedlings were ground to a fine powder in liquid nitrogen and homogenized in 1× PBS buffer supplemented with 0.05% Igepal CA-630 (formerly NP-40), 0.05% Triton, 10 mM NEM, 50 µg ml^{-1} TPCK, 50 µg ml^{-1} TLCK, 0.6 mM PMSF, 100 µM MG132, and 200 µM Phosphate inhibitors cocktail 1 (Sigma). Homogenates were centrifuged at 7674 ***g*** at 4°C for 15 min to remove cellular debris, and the supernatant was further centrifugated at 11 710 ***g*** at 4°C for 3 min before incubation with 15 µl per sample of fresh Halo-Ubiquilin linked to HaloLink™ Resin at 4°C with rotation for 4 h. The resin was washed five times with extraction buffer before elution by boiling in 1× SDS-PAGE sample buffer, including 50 mM DTT.

Western blot

The proteins were separated on 4–20% SDS-PAGE stain-free protein gel (Bio-Rad Laboratories Inc.), followed by transferring onto a *Trans*-Blot® Turbo™ Mini PVDF Transfer Packs (Bio-Rad Laboratories Inc.). For blocking and antibody dilutions, 5% milk powder in Tris-buffered saline was used. For protein detection, the following antibodies were used: monoclonal α-GFP horseradish peroxidase coupled (1 : 5000; Miltenyi Biotech, Bergisch Glad-bach, Germany), α-RFP (1 : 2000; ChromoTek), mouse IgG HRP linked whole antibody (GE Healthcare, Chicago, IL, USA; 1 : 10 000), α-ubiquitin P4D1 (1 : 2500; Millipore), α-GAPDH (1 : 5000; Sigma-Aldrich) and anti-ubiquitinylated proteins antibody, clone FK2 (1 : 1000; Merck, Darmstadt, Germany). Image Lab 6.0 (Bio-Rad, Hercules, CA, USA) was used for protein band quantification. Volume boxes were drawn around the bands of interest in such a way that they include all of the bands with a minimal amount of surrounding background. One mock condition band was set as standard 1. Specific intensities of each band were normalized against the loading control.

Results

Proteome analysis reveals changes in warm temperature-triggered protein levels

Thermoresponsive growth mainly peaks at the beginning and the end of the night period (Box *et al.*, 2015). Therefore, to map proteome changes induced by night-time warm temperature in seedlings, a time-course analysis was performed on Col-0 seedlings that were grown at 21°C under short-day conditions (8 h : 16 h, light : dark) for 7 d and that were subsequently transferred to 21°C (control temperature) or 28°C (warm temperature) at the beginning of the seventh night (Fig. 1a). In this setup, the expression of clock and warm temperature marker genes reflects the warm temperature conditions (Fig. S1; Leivar & Monte, 2014; Zhang *et al.*, 2021a). We collected samples at 15, 30, 120, and 960 min after transfer to 28°C or 21°C to observe changes in protein abundance and protein phosphorylation at early, intermediate, and later stages of the time course. For proteome analysis, we identified 4133 protein groups (Table S2A). We retained proteins that have at least two valid values out of three replicates in at least one time point and one temperature. Through a two-way ANOVA, we identified 93 proteins transiently regulated by temperature (P(time × temperature) < 0.05), 90 proteins mainly affected by temperature alone (P(temperature) < 0.05), and 222 proteins mainly regulated only by time (P(time) < 0.05) (Figs 1b, S2a; Table S2B). Warm temperature leads to 85/90, 87/88, 88/87, and 85/90 up/downregulated proteins after 15, 30, 120, and 960 min, respectively (Table S2C–E). These changes indicated a dynamic regulation of protein abundance during our warm temperature time course. To explore whether the warm temperature proteome was enriched for specific processes, we performed a GO term analysis for biological process and molecular function (Fig. S3). This revealed that chlorophyll and photosynthesis-associated functions are strongly regulated (Fig. S3).

Phosphoproteome analysis identifies warm temperature-dependent phosphorylation of the F-box protein SLOMO

We were particularly interested in ubiquitin-mediated protein degradation machineries that could regulate the observed changes in protein abundance at warm temperature. Since

phosphorylation of E3 ubiquitin ligases affects their activity (Persaud *et al.*, 2014; Perez *et al.*, 2018; Vu *et al.*, 2018a), we used phosphoproteome data that was obtained in parallel to the proteome data to identify possible E3 ligases involved in warm temperature-mediated protein degradation. We identified 10 484 phosphosites mapped onto 7322 phosphopeptides belonging to 3172 phosphoproteins (Table S3A). We performed a two-way ANOVA on 5469 high confidence, reproducibly-quantified phosphosites, which resulted in 353 phosphosites transiently regulated by temperature (P(time × temperature) < 0.05), 802 phosphosites mainly affected by temperature (P(temperature) < 0.05) and 1296 phosphosites mainly regulated by time (P(time) < 0.05) (Figs 1c, S2b; Table S3B). Warm temperature (P(time × temperature) < 0.05) leads to 444/557, 444/557, 467/534, and 455/546 up/downregulated phosphosites and 361/427, 367/434, 382/409, and 362/422 up/downregulated phosphoproteins after 15, 30, 120, and 960 min (Table S3C–E). We also subjected the significant warm temperature-regulated phosphoproteins to a GO analysis for biological process and molecular function (Fig. S4). This revealed, for example processes or functions associated with phosphorylation and kinase activity, mRNA splicing, organelle localization, and endocytosis (Fig. S4). Comparing 712 phosphoproteins with phosphosites showing P(time × temperature) and/or P(temperature) < 0.05 with a list of E3 ligase family members revealed 23 candidates (Fig. 2a; Table S3B,F; Azevedo *et al.*, 2001; Downes *et al.*, 2003; Lee *et al.*, 2008; Xu *et al.*, 2009; Jiménez-López *et al.*, 2018; Vu *et al.*, 2018a; Ban & Estelle, 2021). For further characterization, we selected SLOMO (AT4G33210), an F-box protein and component of an SCF complex (Lohmann *et al.*, 2010), that displayed differential phosphorylation at two serine sites (Fig. 2b,c). The phosphopeptide containing a phosphoserine at position 147 (S147, TVSFGIASSSR) was significantly more abundant over time following transfer to 28°C (Fig. 2b). The abundance of the phosphopeptide containing phosphoserine at position 983 (S983, RVFSSPNLLQD) increased continuously during darkness under control conditions, and was also significantly more present at 28°C (Fig. 2c). These changes can be either due to altered activity of regulatory kinases or phosphatases and/or to elevated levels of the SLOMO protein. Unfortunately, the corresponding proteome dataset for the time course did not identify SLOMO; thus, we cannot fully rule out that overall SLOMO protein levels increased over time and/or at 28°C. The phosphoserine at position 983 is located C-terminal of SLOMO, next to the leucine-rich repeat (LRR) domain and in the substrate specificity-determining domain (Xu *et al.*, 2009; Fig. S5a), and is, together with S984, strongly conserved in dicots and monocots (Fig. S5b). In contrast, the N-terminal region of SLOMO, including S147, is not conserved (Fig. S5a,c). The warm temperature-mediated abundance of phosphorylated SLOMO suggested a role in warm temperature-triggered processes.

SLOMO regulates warm temperature-mediated hypocotyl growth

Using a *pSLOMO::GUS* line (in L*er*) (Lohmann *et al.*, 2010), we found that *SLOMO* is expressed in the hypocotyl at both 21°C and 28°C (Fig. 3a,b). In addition, quantitative real-time reverse transcription PCR (qRT-PCR) revealed a twofold increase in *SLOMO* expression in whole seedlings and in hypocotyls exposed to warm temperature (Fig. 3c,d). To assess SLOMO protein abundance and to confirm the SLOMO phosphorylation sites in seedlings exposed to warm temperature, we used a *slomo-3 pSLOMO::GFP:SLOMO* line (see below). This revealed warm temperature-mediated accumulation of GFP:SLOMO at

28°C (Fig. 3e,f). In addition, following immunoprecipitation mass spectrometry (IP-MS) analysis of GFP:SLOMO, we confirmed the temperature-mediated increase of a SLOMO phosphopeptide containing S983 (Fig. S6). However, this could – at least upon long-term exposure to 28°C – be (partially) due to the increase in SLOMO protein abundance. Furthermore, if only a change in SLOMO protein abundance would be underlying the change in the abundance of phosphorylated SLOMO, then all phosphopeptides should display a similar trend.

The above results prompted us to explore the role of SLOMO in warm temperature-mediated hypocotyl growth. Therefore, we analyzed available T-DNA insertion lines (*slomo-3* (Lohmann *et al.*, 2010) and *slomo-4* (SALK_013287) (Fig. S7a,b), which did not express a full-length *SLOMO* transcript) and a newly generated CRISPR/Cas9-mediated mutant allele with a +G insertion in the first exon and a +T insertion in the second exon which caused a +2 frameshift in the *SLOMO* CDS (*slomo-5*) (Fig. S7a, c). All lines displayed a significantly longer hypocotyl compared with the Col-0 wild-type (WT) when exposed to 21°C or 28°C under both short-day and dark conditions (Figs 4a,b, S8). A two-way ANOVA analysis revealed that there is also a genotype × treatment interaction ($P < 0.01$), indicating a specific role for SLOMO under warm temperature conditions (Figs 4a,b, S8). To further confirm that the loss of *SLOMO* underpinned these phenotypes, we expressed *pSLOMO::GFP:SLOMO* in the *slomo* mutants. Since GFP:SLOMO rescued the hypocotyl elongation growth of *slomo-3* and *slomo-5* plants at both 21°C and 28°C (Figs 4a,b, S9), this indicated that the loss of *SLOMO* was responsible for the hypocotyl length phenotype and that the GFP:SLOMO fusion is functional.

To assess whether phosphorylation at S147 and at S983 is functional, we expressed phosphomutant SLOMO variants tagged with mCherry under the endogenous *SLOMO* promoter (*pSLOMO::mCherry:SLOMO-S147A* or *pSLOMO::mCherry: SLOMO-S983AS984A*) in the *slomo-5* mutant. We selected two representative lines with detectable mCherry:SLOMO levels for both phosphomutant SLOMO variants (Fig. S10). The phosphomutant SLOMO variants could not rescue the *slomo-5* hypocotyl phenotype (Fig. 4c–e). Taken together, our data indicate that SLOMO plays role in warm temperature-mediated signaling and that phosphorylation at S147 and S983 is vital for SLOMO activity.

SLOMO interacts with a wide range of proteins

Because SLOMO is an F-box protein, we first investigated whether loss of SLOMO function affects the total cellular level of ubiquitin conjugates. To examine this, we utilized Halo-Ubiquilin tandem ubiquitin-binding entities that pull down ubiquitin chains and ubiquitinated substrates with high affinity (Hjerpe *et al.*, 2009). Indeed, compared with WT, *slomo* mutants accumulated fewer ubiquitin conjugates, suggesting SLOMO targets a substantial number of substrates for degradation (Figs 5, S11). Next, to identify interactors and putative substrates of SLOMO, we used a SLOMO-decoy approach to stabilize E3-targets interaction for the following detection (Lohmann *et al.*, 2010; Lee *et al.*, 2018; Feke *et al.*, 2019). The SLOMO-decoy protein, which lacks the F-box domain, is still able to bind to substrates but lacks the ability to be recruited into CULLIN 1 ligase complexes to mediate substrate ubiquitination and degradation. We generated a stable *Arabidopsis* line expressing

35S:: GFP:SLOMO-Decoy and performed IP-MS analysis on GFP: SLOMO-Decoy. We subsequently retained (putative) interactors based on a stringent criterium (only detected in at least 3 out of 4 GFP:SLOMO-Decoy biological replicates and not in the control samples) or being significantly enriched in the GFP:SLOMO-Decoy samples vs the control samples (Table S4). We identified six heat shock proteins (HSPs), some of which may act as F-box regulatory partners (Kim *et al.*, 2011; He *et al.*, 2012; Wang *et al.*, 2016), and 200 other putative interactors, including the hypocotyl growth or temperature response-associated proteins PHOTOTROPIN 1 (PHOT1), PROTEIN PHOSPHATASE 2A SUBUNIT A2 (PP2AA2) (Liu *et al.*, 2022), MITOGEN-ACTIVATED PROTEIN KINASE KINASE 5 (MKK5) (C. Zhao *et al.*, 2017), NINE-*CIS*-EPOXYCAROTENTENOID DIOXYGENASE 4 (NCED4) (Huo *et al.*, 2013), GLYCO-LATE OXIDASE 1 (GOX1), UBIQUITIN-SPECIFIC PROTEASE 12 (UBP12), and UBP13 (Zhou *et al.*, 2021; Table S4).

To validate our interactome dataset, we performed co-IPs on transiently co-expressed mCherry-SLOMO or mCherry-SLOMO-Decoy with two selected candidates with distinct functions, namely MKK5 (a kinase) or NCED4 (an ABA synthesis enzyme). We confirmed the interactions between SLOMO and MKK5 or NCED4 (Fig. 6), increasing confidence in the co-IP data. We reasoned that SLOMO interactors could be novel regulators of (warm temperature-mediated) hypocotyl growth. Indeed, a loss-of-function line of the hormone biosynthesis enzyme NCED4 displayed a subtle hypocotyl growth phenotype at 28°C (Fig. S12a,b). In contrast, a loss-of-function line of the kinase MKK5 did not display a hypocotyl growth phenotype (Fig. S12c,d), which could be due to redundancy with MKK4 (M. Zhang *et al.*, 2017) or MKK5 is involved in so far unknown SLOMO roles. In addition, we also explored whether PHOTOTROPIN 1 (PHOT1), a blue-light photoreceptor involved in hypocotyl phototropism (Christie, 2007; Q.-P. Zhao *et al.*, 2017) and another putative SLOMO-interacting protein, is also involved in warm temperature-mediated hypocotyl growth. However, in our hands, a *phot1* mutant did not display an obvious hypocotyl growth phenotype at 21°C or 28°C (Fig. S12e,f).

DWF1 is a likely SLOMO substrate

To further narrow down putative SLOMO substrates, we compared the list of putative SLOMO interactors with a list of proteins of which the abundance changes in the (warm temperature) time course (Fig. 7a; Table S5), which are thus likely targets for SLOMO-mediated degradation. As we do not know whether SLOMO phosphorylation leads to its activation or inactivation, we included both proteins with increased or decreased abundance. There are 31 candidates of which the protein level was regulated by warm temperature and which are putative SLOMO interactors, including PHE AMMONIA LYASE 1 (PAL1), PATELLIN 2 (PATL2), HEAT SHOCK PROTEIN 70 (HSP70), UBP12, and DWARF1 (DWF1) (Fig. 7a; Table S5).

We focused on DWF1 (Fig. 7b), an important protein for brassinosteroid (BR) biosynthesis, cell elongation, and hypocotyl growth (Takahashi *et al.*, 1995; Klahre *et al.*, 1998; Youn *et al.*, 2018). Furthermore, BR plays an important role in thermomorphogenesis (Ibañez *et al.*, 2018) and PIF4-induced BR synthesis is critical for diurnal and thermomorphogenic growth (Martínez *et al.*, 2018). We next showed that DWF1 is ubiquitinated and that ubiquitinated

DWF1 accumulated if proteasome-mediated protein degradation was inhibited (Figs 7c,d, S13). Through a co-IP on transiently co-expressed mCherry-SLOMO or mCherry-SLOMO-Decoy with GFP-tagged DWF1, we then confirmed the interaction between SLOMO and DWF1 (Fig. 7e). The interaction between SLOMO and DWF1 was not affected in the phosphomutant SLOMO variants (Fig. S14). However, compared with SLOMO, the phosphomutant SLOMO variants slightly affected the abundance of ubiquitinated DWF1 (Fig. S14). Next, we generated a *35S::DWF1:YFP slomo-5* line, and we observed that the DWF1-YFP protein accumulated to a lower level in the *slomo* mutant compared with the *35S::DWF1:YFP* control line (Figs 8a, S15). This is possibly due to a lower expression of *DWF1:YFP* (Fig. S15) or another regulatory mechanism downstream of SLOMO. Nevertheless, we observed that the warm temperature-mediated reduction of DWF1:YFP is absent in *35S::DWF1:YFP slomo-5* compared with the *35S::DWF1:YFP* line (Figs 8a,b, S15). In addition, we transiently co-expressed mCherry:SLOMO and GFP:DWF1 in tobacco and this revealed lower GFP:DWF1 levels in the presence of SLOMO (Fig. 8c,d). Finally, *dwf1* (Choe *et al.*, 1999; Du & Poovaiah, 2005) and *slomo-3 dwf1* mutants displayed a warm temperature-mediated hypocotyl length phenotype (Fig. 9a,b). Taken together, the SLOMO–DWF1 interaction, the ubiquitination of DWF1, the reduced DWF1 protein levels at warm temperature, and the *dwf1* phenotype support a role for DWF1 in thermomorphogenesis and suggest that DWF1 is a likely substrate of SLOMO.

Discussion

With increasing global warming, plants need to cope even more with warm temperature-induced stress. One important response to warm temperature is a longer hypocotyl, which contributes to cooling of the plants (Vu *et al.*, 2019). While several key regulators of this process have been identified (Quint *et al.*, 2016; Delker *et al.*, 2022), the role of post-translational modifications (PTMs) and protein abundance in this process has hardly been investigated. During post-translational modification of a protein, a small molecule is added to modify, for example the location, stability or function of target proteins, which is vital for survival in acute stress situations because it enables a swift response to a changing environment (Malini *et al.*, 2020). Recent studies demonstrated that various PTMs, like sumoylation, histone methylation, and acetylation, occur in response to warm temperature and high temperature stress (Han *et al.*, 2022). Ubiquitination leads to protein degradation (Hershko & Ciechanover, 1998), and this is likely a very important mechanism to control warm temperature-mediated responses.

Our proteome results revealed that the abundance of nearly 100 proteins is affected by warm temperature treatment over time. Activation of E3 ligases is a major mechanism to regulate protein abundance, and phosphorylation of E3 ligases influences their activity (Vu *et al.*, 2018a). We found that the F-box protein SLOMO displays differential phosphorylation at Serine147 and Serine983 following a warm temperature treatment. Since *SLOMO* is expressed throughout the seedling, it likely has multiple functions in plant growth and development. For example, *slomo* mutants display a delay in lateral organ initiation without affecting other aspects of shoot meristem function (Lohmann *et al.*, 2010). In addition, SLOMO regulates warm temperature-mediated hypocotyl growth, and our IP-MS analyses detected 206 putative SLOMO interactors, including probable substrates, associated with

different biological processes. Among them, NCED4 and MKK5 are involved in ABA and MAPK signaling, respectively (Nambara & Marion-Poll, 2005; Xing *et al.*, 2015). The mitogen-activated protein kinase (MAPK) cascade is one of most highly conserved signaling pathways for signal transduction in eukaryotes (Xing *et al.*, 2015), and MKK5 functions in MAPK cascades regulating, for example plant immune response, hydrogen peroxide production and leaf senescence (Asai *et al.*, 2002; Ren *et al.*, 2002; Gao *et al.*, 2008; Zhang *et al.*, 2020). As SLOMO was identified in a phosphoproteome analysis and its phosphorylation may be important for its function, we speculate that MKK5 might act as a regulatory kinase. However, given the lack of an *mkk5* hypocotyl phenotype, which could be due to redundancy with MKK4 (M. Zhang *et al.*, 2017), this is only a hypothesis. With respect to NCED4, which is involved in ABA hormone biosynthesis (Nambara & Marion-Poll, 2005) and essential for thermo-inhibition of lettuce (*Lactuca sativa*) seed germination (Huo *et al.*, 2013), the loss-of-function *nced4* mutant shows a longer hypocotyl compared with Col-0 under warm temperature treatment. Taken together, the interaction of NCED4 and SLOMO suggests a role for SLOMO in ABA-mediated signaling.

Brassinosteroids (BR) protect crop yields through amplifying responses to heat stress and rescuing the expression of growth promoters (Kothari & Lachowiec, 2021). Brassinosteroid acts downstream of the central thermomorphogenesis regulator PIF4 and regulates hypocotyl growth via the direct interaction of PIF4 and BRASSINAZOLE RESISTANT 1 (BZR1) (Ibañez *et al.*, 2018). Our work revealed another control point on BR signaling in response to warm temperature (Fig. 10), namely the F-box protein SLOMO interacting with the BR biosynthesis enzyme DWF1, thereby ubiquitinating DWF1 and inducing its degradation (Figs 7, 8). We propose that warm temperature-mediated regulation of SLOMO activity controls the abundance of hypocotyl growth regulators, such as DWF1, through ubiquitin-mediated degradation. Indeed, loss of DWF1 induces a BR-deficient compact plant phenotype (Youn *et al.*, 2018). In contrast, the *slomo* mutant presents a longer hypocotyl (Fig. 4), possibly reflecting the accumulation of endogenous BR leading to increased growth (Fig. 10).

Supplementary Material

Refer to Web version on PubMed Central for supplementary material.

Acknowledgements

We thank Michael Lenhard for the *pSLOMO::GUS* seeds, Wolf-gang Lukowitz for the *mkk5-18* seeds and Marnik Vuylsteke for statistical analysis of the proteome and phosphoproteome. LP, XX, SZ, and TZ were supported by the Chinese Scholarship Council (201806870020, 201706350153, 201506230173, and 201706910095); XX and LP received support from the Ghent University Special Research Fund (01CD7122 and 01CD0523); LDV was funded through a postdoctoral fellowship of the Ghent University Special Research Fund (01P12219); and TZ is supported by a postdoctoral research mandate from the Ghent University Special Research Fund (01P11322).

Data availability

All data included in this study are available as Supporting Information. MS data are available via ProteomeXchange with identifiers PXD035922 and PXD028319.

References

Asai T, Tena G, Plotnikova J, Willmann MR, Chiu W-L, Gomez-Gomez L, Boller T, Ausubel FM, Sheen J. 2002. MAP kinase signalling cascade in Arabidopsis innate immunity. Nature 415: 977–983. [PubMed: 11875555]

Azevedo C, Santos-Rosa MJ, Shirasu K. 2001. The U-box protein family in plants. Trends in Plant Science 6: 354–358. [PubMed: 11495788]

Balaji V, Hoppe T. 2020. Regulation of E3 ubiquitin ligases by homotypic and heterotypic assembly. F1000Research 9: 88.

Ban Z, Estelle M. 2021. CUL3 E3 ligases in plant development and environmental response. Nature Plants 7: 6–16. [PubMed: 33452490]

Box MS, Huang BE, Domijan M, Jaeger KE, Khattak AK, Yoo SJ, Sedivy EL, Jones DM, Hearn TJ, Webb AAR et al. 2015. ELF3 controls thermoresponsive growth in Arabidopsis. Current Biology 25: 194–199. [PubMed: 25557663]

Brinkman EK, Chen T, Amendola M, van Steensel B. 2014. Easy quantitative assessment of genome editing by sequence trace decomposition. Nucleic Acids Research 42: e168. [PubMed: 25300484]

Bulatov E, Ciulli A. 2015. Targeting Cullin–RING E3 ubiquitin ligases for drug discovery: structure, assembly and small-molecule modulation. Biochemical Journal 467: 365–386. [PubMed: 25886174]

Casal JJ, Balasubramanian S. 2019. Thermomorphogenesis. Annual Review of Plant Biology 70: 321–346.

Castroverde CDM, Dina D. 2021. Temperature regulation of plant hormone signaling during stress and development. Journal of Experimental Botany 70: 7436–7458.

Chen L, Hellmann H. 2013. Plant E3 ligases: flexible enzymes in a sessile world. Molecular Plant 6: 1388–1404. [PubMed: 23307436]

Chiu RS, Pan S, Zhao R, Gazzarrini S. 2016. ABA-dependent inhibition of the ubiquitin proteasome system during germination at high temperature in Arabidopsis. The Plant Journal 88: 749–761. [PubMed: 27496613]

Choe S, Dilkes BP, Gregory BD, Ross AS, Yuan H, Noguchi T, Fujioka S, Takatsuto S, Tanaka A, Yoshida S et al. 1999. The Arabidopsis dwarf1 mutant is defective in the conversion of 24-methylenecholesterol to campesterol in brassinosteroid biosynthesis1. Plant Physiology 119: 897–908. [PubMed: 10069828]

Christie JM. 2007. Phototropin blue-light receptors. Annual Review of Plant Biology 58: 21–45.

Chung BYW, Balcerowicz M, Di Antonio M, Jaeger KE, Geng F, Franaszek K, Marriott P, Brierley I, Firth AE, Wigge PA. 2020. An RNA thermoswitch regulates daytime growth in Arabidopsis. Nature Plants 6: 522–532. [PubMed: 32284544]

Clough SJ, Bent AF. 1998. Floral dip: a simplified method for *Agrobacterium*-mediated transformation of *Arabidopsis thaliana*. The Plant Journal 16: 735–743. [PubMed: 10069079]

Cox J, Hein MY, Luber CA, Paron I, Nagaraj N, Mann M. 2014. Accurate proteome-wide label-free quantification by delayed normalization and maximal peptide ratio extraction, termed MaxLFQ. Molecular & Cellular Proteomics 13: 2513–2526. [PubMed: 24942700]

Decaestecker W, Buono RA, Pfeiffer ML, Vangheluwe N, Jourquin J, Karimi M, Van Isterdael G, Beeckman T, Nowack MK, Jacobs TB. 2019. CRISPR-TSKO: a technique for efficient mutagenesis in specific cell types, tissues, or organs in Arabidopsis. Plant Cell 31: 2868–2887. [PubMed: 31562216]

Delker C, Quint M, Wigge PA. 2022. Recent advances in understanding thermomorphogenesis signaling. Current Opinion in Plant Biology 68: 102231. [PubMed: 35636376]

Delker C, Sonntag L, James GV, Janitza P, Ibañez C, Ziermann H, Peterson T, Denk K, Mull S, Ziegler J et al. 2014. The DET1-COP1-HY5 pathway constitutes a multipurpose signaling module regulating plant photomorphogenesis and thermomorphogenesis. Cell Reports 9: 1983–1989. [PubMed: 25533339]

Downes BP, Stupar RM, Gingerich DJ, Vierstra RD. 2003. The HECT ubiquitin-protein ligase (UPL) family in Arabidopsis: UPL3 has a specific role in trichome development. The Plant Journal 35: 729–742. [PubMed: 12969426]

Du L, Poovaiah BW. 2005. Ca^{2+}/calmodulin is critical for brassinosteroid biosynthesis and plant growth. Nature 437: 741–745. [PubMed: 16193053]

Feke A, Liu W, Hong J, Li M-W, Lee C-M, Zhou EK, Gendron JM. 2019. Decoys provide a scalable platform for the identification of plant E3 ubiquitin ligases that regulate circadian function. eLife 8: e44558. [PubMed: 30950791]

Gangappa SN, Kumar SV. 2017. DET1 and HY5 control PIF4-mediated thermosensory elongation growth through distinct mechanisms. Cell Reports 18: 344–351. [PubMed: 28076780]

Gao M, Liu J, Bi D, Zhang Z, Cheng F, Chen S, Zhang Y. 2008. MEKK1, MKK1/MKK2 and MPK4 function together in a mitogen-activated protein kinase cascade to regulate innate immunity in plants. Cell Research 18: 1190–1198. [PubMed: 18982020]

Han D, Yu Z, Lai J, Yang C. 2022. Post-translational modification: a strategic response to high temperature in plants. aBIOTECH 3: 49–64. [PubMed: 36304199]

He Y, Chung E-H, Hubert DA, Tornero P, Dangl JL. 2012. Specific missense alleles of the Arabidopsis jasmonic acid co-receptor COI1 regulate innate immune receptor accumulation and function. PLoS Genetics 8: e1003018. [PubMed: 23093946]

Hershko A, Ciechanover A. 1998. The ubiquitin system. Annual Review of Biochemistry 67: 425–479.

Hjerpe R, Aillet F, Lopitz-Otsoa F, Lang V, England P, Rodriguez MS. 2009. Efficient protection and isolation of ubiquitylated proteins using tandem ubiquitin-binding entities. EMBO Reports 10: 1250–1258. [PubMed: 19798103]

Huo H, Dahal P, Kunusoth K, McCallum CM, Bradford KJ. 2013. Expression of 9-cis-EPOXYCAROTENOID DIOXYGENASE4 is essential for thermoinhibition of lettuce seed germination but not for seed development or stress tolerance. Plant Cell 25: 884–900. [PubMed: 23503626]

Ibañez C, Delker C, Martinez C, Bürstenbinder K, Janitza P, Lippmann R, Ludwig W, Sun H, James GV, Klecker M et al. 2018. Brassinosteroids dominate hormonal regulation of plant thermomorphogenesis via BZR1. Current Biology 28: 303–310. [PubMed: 29337075]

Jiménez-López D, Muñóz-Belman F, González-Prieto JM, Aguilar-Hernández V, Guzmán P. 2018. Repertoire of plant RING E3 ubiquitin ligases revisited: new groups counting gene families and single genes. PLoS ONE 13: e0203442. [PubMed: 30169501]

Jin H, Zhu Z. 2019. Dark, light, and temperature: key players in plant morphogenesis. Plant Physiology 180: 1793–1802. [PubMed: 31113832]

Josse E-M, Halliday KJ. 2008. Skotomorphogenesis: the dark side of light signalling. Current Biology 18: R1144–R1146. [PubMed: 19108774]

Karimi M, Inzé D, Depicker A. 2002. GATEWAY™ vectors for *Agrobacterium*-mediated plant transformation. Trends in Plant Science 7: 193–195. [PubMed: 11992820]

Kim T-S, Kim WY, Fujiwara S, Kim J, Cha J-Y, Park JH, Lee SY, Somers DE. 2011. HSP90 functions in the circadian clock through stabilization of the client F-box protein ZEITLUPE. Proceedings of the National Academy of Sciences, USA 108: 16843–16848.

Kinoshita T, Doi M, Suetsugu N, Kagawa T, Wada M, Shimazaki K. 2001. phot1 and phot2 mediate blue light regulation of stomatal opening. Nature 414: 656–660. [PubMed: 11740564]

Klahre U, Noguchi T, Fujioka S, Takatsuto S, Yokota T, Nomura T, Yoshida S, Chua N-H. 1998. The Arabidopsis DIMINUTO/DWARF1 gene encodes a protein involved in steroid synthesis. Plant Cell 10: 1677–1690. [PubMed: 9761794]

Kothari A, Lachowiec J. 2021. Roles of brassinosteroids in mitigating heat stress damage in cereal crops. International Journal of Molecular Sciences 22: 2706. [PubMed: 33800127]

Lee C-M, Feke A, Li M-W, Adamchek C, Webb K, Pruneda-Paz J, Bennett EJ, Kay SA, Gendron JM. 2018. Decoys untangle complicated redundancy and reveal targets of circadian clock F-box proteins. Plant Physiology 177: 1170–1186. [PubMed: 29794020]

Lee J-H, Terzaghi W, Gusmaroli G, Charron J-BF, Yoon H-J, Chen H, He YJ, Xiong Y, Deng XW. 2008. Characterization of Arabidopsis and rice DWD proteins and their roles as substrate receptors for CUL4-RING E3 ubiquitin ligases. Plant Cell 20: 152–167. [PubMed: 18223036]

Leivar P, Monte E. 2014. PIFs: systems integrators in plant development. Plant Cell 26: 56–78. [PubMed: 24481072]

Li N, Euring D, Cha JY, Lin Z, Lu M, Huang L-J, Kim WY. 2021. Plant hormone-mediated regulation of heat tolerance in response to global climate change. Frontiers in Plant Science 11: 627969. [PubMed: 33643337]

Liu H, Lu Y, Wang X, Wang X, Li R, Lu C, Lan X, Chen Y. 2022. Selection and validation of reference genes for RT-qPCR analysis in Tibetan medicinal plant *Saussurea laniceps* callus under abiotic stresses and hormone treatments. Genes 13: 904. [PubMed: 35627289]

Liu Y, Xiao S, Sun H, Pei L, Liu Y, Peng L, Gao X, Liu Y, Wang J. 2020. AtPPRT1, an E3 ubiquitin ligase, enhances the thermotolerance in Arabidopsis. Plants 9: 1074. [PubMed: 32825569]

Lohmann D, Stacey N, Breuninger H, Jikumaru Y, Müller D, Sicard A, Leyser O, Yamaguchi S, Lenhard M. 2010. SLOW MOTION is required for within-plant auxin homeostasis and normal timing of lateral organ initiation at the shoot meristem in Arabidopsis. Plant Cell 22: 335–348. [PubMed: 20139162]

Malini MK, Lekshmy VS, Pal M, Chinnusamy V, Kumar MN. 2020. Unfolded protein response (UPR) mediated under heat stress in plants. Plant Physiology Reports 25: 569–582.

Martínez C, Espinosa-Ruíz A, de Lucas M, Bernardo-García S, Franco-Zorrilla JM, Prat S. 2018. PIF4-induced BR synthesis is critical to diurnal and thermomorphogenic growth. EMBO Journal 37: e99552. [PubMed: 30389669]

Morimoto K, Ohama N, Kidokoro S, Mizoi J, Takahashi F, Todaka D, Mogami J, Sato H, Qin F, Kim J-S et al. 2017. BPM-CUL3 E3 ligase modulates thermotolerance by facilitating negative regulatory domain-mediated degradation of DREB2A in Arabidopsis. Proceedings of the National Academy of Sciences, USA 114: E8528–E8536.

Nambara E, Marion-Poll A. 2005. Abscisic acid biosynthesis and catabolism. Annual Review of Plant Biology 56: 165–185.

Ohama N, Sato H, Shinozaki K, Yamaguchi-Shinozaki K. 2016. Transcriptional regulatory network of plant heat stress response. Trends in Plant Science 22: 53–65. [PubMed: 27666516]

Park Y-J, Lee H-J, Ha J-H, Kim JY, Park C-M. 2017. COP1 conveys warm temperature information to hypocotyl thermomorphogenesis. New Phytologist 215: 269–280. [PubMed: 28418582]

Peng L, Wan X, Huang K, Pei L, Xiong J, Li X, Wang J. 2019. AtPUB48 E3 ligase plays a crucial role in the thermotolerance of Arabidopsis. Biochemical and Biophysical Research Communications 509: 281–286. [PubMed: 30591216]

Perez JM, Chen Y, Xiao TS, Abbott DW. 2018. Phosphorylation of the E3 ubiquitin protein ligase ITCH diminishes binding to its cognate E2 ubiquitin ligase. The Journal of Biological Chemistry 293: 1100–1105. [PubMed: 29212706]

Perez-Riverol Y, Csordas A, Bai J, Bernal-Llinares M, Hewapathirana S, Kundu DJ, Inuganti A, Griss J, Mayer G, Eisenacher M et al. 2019. The PRIDE database and related tools and resources in 2019: improving support for quantification data. Nucleic Acids Research 47: D442–D450. [PubMed: 30395289]

Persaud A, Alberts P, Mari S, Tong J, Murchie R, Maspero E, Safi F, Moran MF, Polo S, Rotin D. 2014. Tyrosine phosphorylation of NEDD4 activates its ubiquitin ligase activity. Science Signaling 7: ra95. [PubMed: 25292214]

Praat M, De Smet I, van Zanten M. 2021. Protein kinase and phosphatase control of plant temperature responses. Journal of Experimental Botany 72: 7459–7473.

Qiu Y, Li M, Kim RJ-A, Moore CM, Chen M. 2019. Daytime temperature is sensed by phytochrome B in Arabidopsis through a transcriptional activator HEMERA. Nature Communications 10: 140.

Quint M, Delker C, Franklin KA, Wigge PA, Halliday KJ, van Zanten M. 2016. Molecular and genetic control of plant thermomorphogenesis. Nature Plants 2: 15190. [PubMed: 27250752]

Ren D, Yang H, Zhang S. 2002. Cell death mediated by MAPK is associated with hydrogen peroxide production in Arabidopsis. Journal of Biological Chemistry 277: 559–565. [PubMed: 11687590]

Rottet S, Devillers J, Glauser G, Douet V, Besagni C, Kessler F. 2016. Identification of plastoglobules as a site of carotenoid cleavage. Frontiers in Plant Science 7: 1855. [PubMed: 28018391]

Silvestro D, Andersen TG, Schaller H, Jensen PE. 2013. Plant sterol metabolism. Δ7-sterol-C5-desaturase (STE1/DWARF7), Δ5,7-sterol-Δ7-reductase (DWARF5) and Δ24-sterol-Δ24-reductase (DIMINUTO/DWARF1) show multiple subcellular localizations in *Arabidopsis thaliana* (Heynh) L. PLoS ONE 8: e56429. [PubMed: 23409184]

Takahashi T, Gasch A, Nishizawa N, Chua NH. 1995. The DIMINUTO gene of Arabidopsis is involved in regulating cell elongation. Genes & Development 9: 97–107. [PubMed: 7828854]

Tasset C, Singh Yadav A, Sureshkumar S, Singh R, van der Woude L, Nekrasov M, Tremethick D, van Zanten M, Balasubramanian S. 2018. POWERDRESS-mediated histone deacetylation is essential for thermomorphogenesis in *Arabidopsis thaliana*. PLoS Genetics 14: e1007280. [PubMed: 29547672]

Till BJ, Reynolds SH, Greene EA, Codomo CA, Enns LC, Johnson JE, Burtner C, Odden AR, Young K, Taylor NE et al. 2003. Large-scale discovery of induced point mutations with high-throughput TILLING. Genome Research 13: 524–530. [PubMed: 12618384]

Van Bel M, Diels T, Vancaester E, Kreft L, Botzki A, Van de Peer Y, Coppens F, Vandepoele K. 2018. PLAZA 4.0: an integrative resource for functional, evolutionary and comparative plant genomics. Nucleic Acids Research 46: D1190–D1196. [PubMed: 29069403]

Vu LD, Gevaert K, De Smet I. 2018a. Protein language: post-translational modifications talking to each other. Trends in Plant Science 23: 1068–1080. [PubMed: 30279071]

Vu LD, Stes E, Van Bel M, Nelissen H, Maddelein D, Inzé D, Coppens F, Martens L, Gevaert K, De Smet I. 2016. Up-to-date workflow for plant (phospho)proteomics identifies differential drought-responsive phosphorylation events in maize leaves. Journal of Proteome Research 15: 4304–4317. [PubMed: 27643528]

Vu LD, Xu X, Gevaert K, De Smet I. 2019. Developmental plasticity at high temperature. Plant Physiology 181: 399–411. [PubMed: 31363006]

Vu LD, Xu X, Zhu T, Pan L, van Zanten M, de Jong D, Wang Y, Vanremoortele T, Locke AM, van de Cotte B et al. 2021. The membrane-localized protein kinase MAP4K4/TOT3 regulates thermomorphogenesis. Nature Communications 12: 2842.

Vu LD, Zhu T, Verstraeten I, van de Cotte B, Gevaert K, De Smet I. 2018b. Temperature-induced changes in the wheat phosphoproteome reveal temperature-regulated interconversion of phosphoforms. Journal of Experimental Botany 69: 4609–4624. [PubMed: 29939309]

Wang R, Zhang Y, Kieffer M, Yu H, Kepinski S, Estelle M. 2016. HSP90 regulates temperature-dependent seedling growth in Arabidopsis by stabilizing the auxin co-receptor F-box protein TIR1. Nature Communications 7: 10269.

Xing Y, Chen W, Jia W, Zhang J. 2015. Mitogen-activated protein kinase kinase 5 (MKK5)-mediated signalling cascade regulates expression of iron superoxide dismutase gene in Arabidopsis under salinity stress. Journal of Experimental Botany 66: 5971–5981. [PubMed: 26136265]

Xu G, Ma H, Nei M, Kong H. 2009. Evolution of F-box genes in plants: different modes of sequence divergence and their relationships with functional diversification. Proceedings of the National Academy of Sciences, USA 106: 835–840.

Xue M, Zhang H, Zhao F, Zhao T, Li H, Jiang D. 2021. The INO80 chromatin remodeling complex promotes thermomorphogenesis by connecting H2A.Z eviction and active transcription in Arabidopsis. Molecular Plant 14: 1799–1813. [PubMed: 34242850]

Youn JH, Kim T-W, Joo S-H, Son S-H, Roh J, Kim S, Kim T-W, Kim S-K. 2018. Function and molecular regulation of DWARF1 as a C-24 reductase in brassinosteroid biosynthesis in Arabidopsis. Journal of Experimental Botany 69: 1873–1886. [PubMed: 29432595]

Zhang B, Holmlund M, Lorrain S, Norberg M, Bakó L, Fankhauser C, Nilsson O. 2017. BLADE-ON-PETIOLE proteins act in an E3 ubiquitin ligase complex to regulate PHYTOCHROME INTERACTING FACTOR 4 abundance. eLife 6: e26759. [PubMed: 28826468]

Zhang J, Gao J, Zhu Z, Song Y, Wang X, Wang X, Zhou X. 2020. MKK4/MKK5-MPK1/MPK2 cascade mediates SA-activated leaf senescence via phosphorylation of NPR1 in Arabidopsis. Plant Molecular Biology 102: 463–475. [PubMed: 31916083]

Zhang LL, Luo A, Davis SJ, Liu J-X. 2021a. Timing to grow: roles of clock in thermomorphogenesis. Trends in Plant Science 26: 1248–1257. [PubMed: 34404586]

Zhang LL, Shao YJ, Ding L, Wang MJ, Davis SJ, Liu JX. 2021b. XBAT31 regulates thermoresponsive hypocotyl growth through mediating degradation of the thermosensor ELF3 in Arabidopsis. Science Advances 7: eabf4427. [PubMed: 33962946]

Zhang M, Wu H, Su J, Wang H, Zhu Q, Liu Y, Xu J, Lukowitz W, Zhang S. 2017. Maternal control of embryogenesis by MPK6 and its upstream MKK4/MKK5 in Arabidopsis. The Plant Journal 92: 1005–1019. [PubMed: 29024034]

Zhao C, Wang P, Si T, Hsu C-C, Wang L, Zayed O, Yu Z, Zhu Y, Dong J, Tao WA et al. 2017. MAP kinase cascades regulate the cold response by modulating ICE1 protein stability. Developmental Cell 43: 618–629. [PubMed: 29056551]

Zhao Q-P, Zhao X, Zhu Z-Y, Guo X, Li N-N, Zhang X. 2017. Isolation and characterization of regulators involved in PHOT1-mediated inhibition of hypocotyl phototropism in Arabidopsis. Biologia 72: 601–607.

Zhou Y, Park S-H, Soh MY, Chua N-H. 2021. Ubiquitin-specific proteases UBP12 and UBP13 promote shade avoidance response by enhancing PIF7 stability. Proceedings of the National Academy of Sciences, USA 118: e2103633118.

Zhu T, Herrfurth C, Xin M, Savchenko T, Feussner I, Goossens A, De Smet I. 2021. Warm temperature triggers JOX and ST2A-mediated jasmonate catabolism to promote plant growth. Nature Communications 12: 4804.

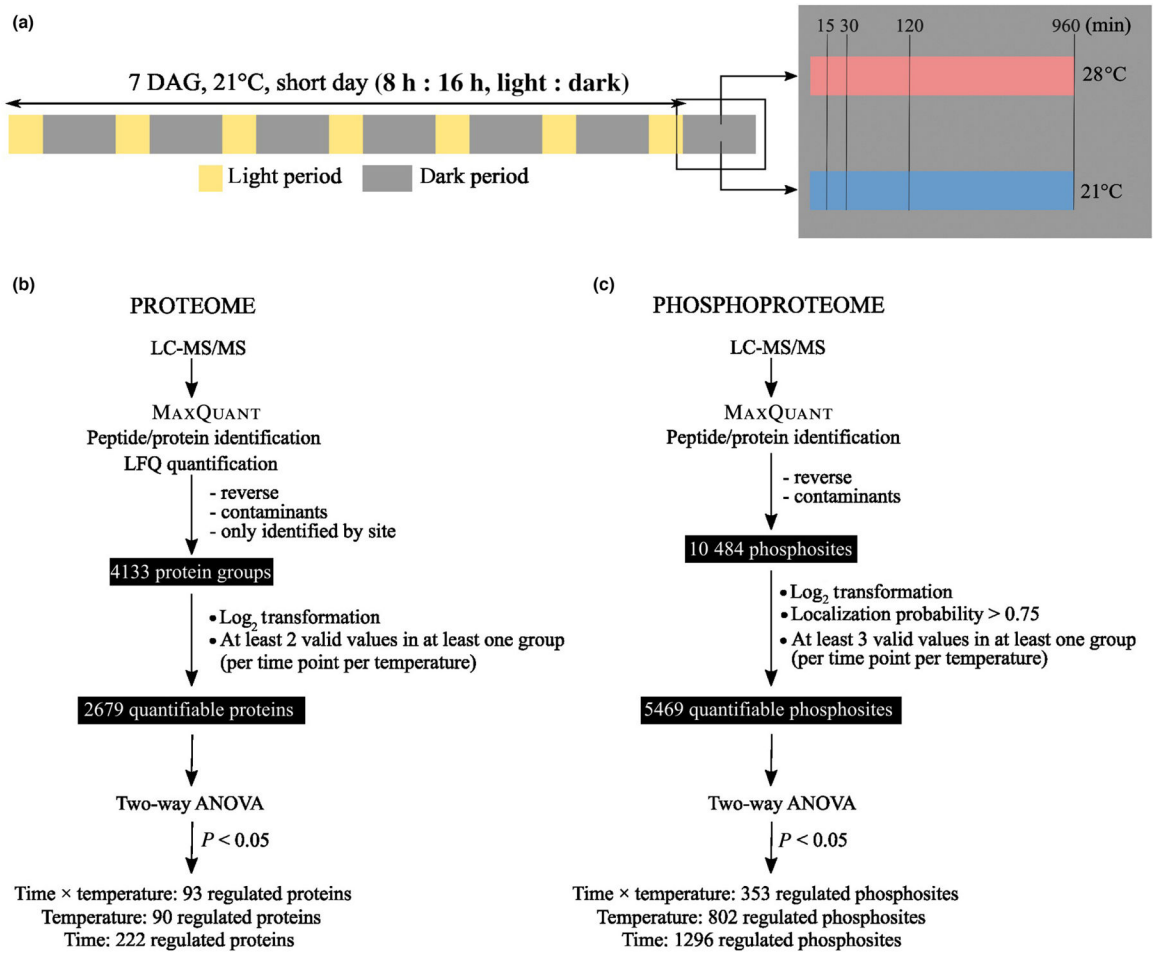

Fig. 1.

Phosphoproteome and proteome analysis of *Arabidopsis thaliana* exposed to different temperatures. (a) Experimental setup for plant growth, treatment of seedlings at 21°C and 28°C, and time points for sampling. (b) Summary of the proteome analysis of *Arabidopsis* exposed to 21°C and 28°C. (c) Summary of the phosphoproteome analysis of *Arabidopsis* seedlings exposed to 21°C and 28°C.

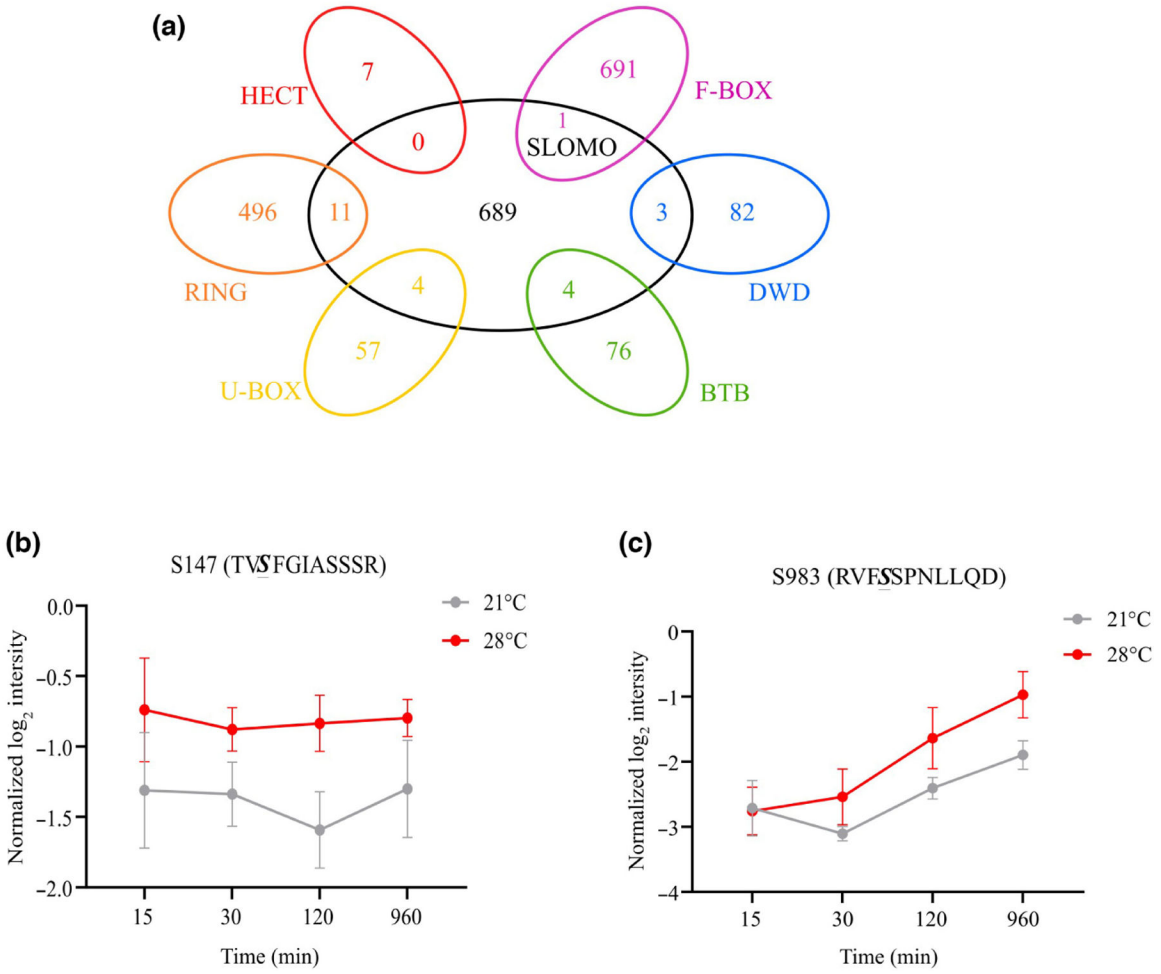

Fig. 2.

Phosphorylation of the E3 ligase SLOMO is deregulated by high temperature. (a) Venn diagram showing the overlapping of different E3 ligase family members and phosphoproteins deregulated by high temperature. (b, c) The SLOMO residues S147 (b) and S983 (c) are deregulated at 28°C.

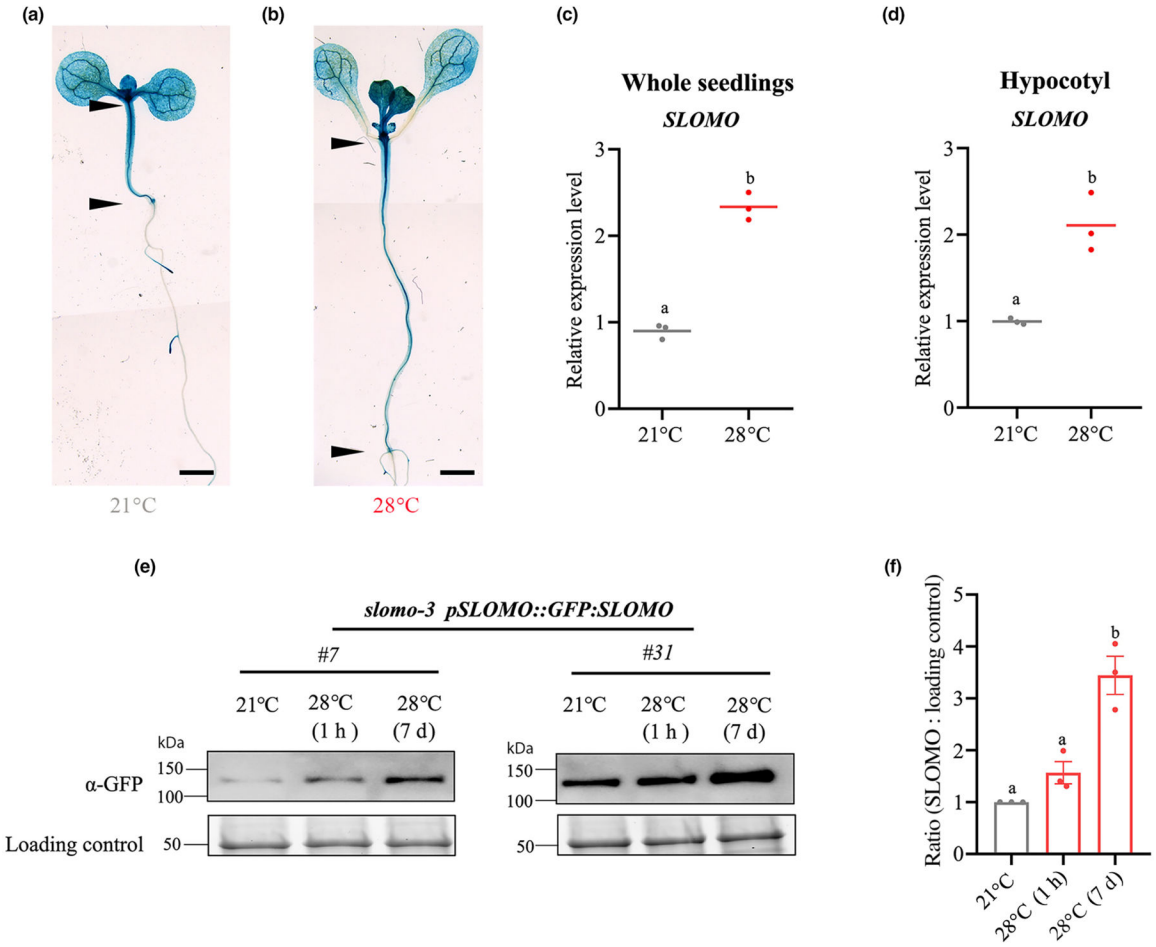

Fig. 3.

SLOMO expression is elevated at warm temperature in *Arabidopsis thaliana*. (a, b) *SLOMO* expression in 7-d-old *pSLOMO::GUS* L*er* seedlings grown at 21°C (a) or 28°C (b). The hypocotyl is marked between two arrowheads. Bars, 2 mm. (c, d) *SLOMO* expression in 7-d-old whole Col-0 seedlings (c) or hypocotyl (d) grown at 21°C and 28°C as determined by RT-qPCR. Graph shows average (line) of three biological replicates (shown as dots). Letters indicate significant differences based on one-way ANOVA and Tukey's test ($P < 0.05$). (e, f) SLOMO protein abundance upon high temperature treatment. Representative images of GFP:SLOMO levels in 7-d-old *slomo-3 pSLOMO::GPF:SLOMO* seedlings continuously grown at 21°C and 28°C or 7-d-old seedlings grown at 21°C then transferred to 28°C for 1 h, as revealed through western blot of two independent *slomo-3 pSLOMO::GPF:SLOMO* lines. Total protein extracts probed with α-GFP antibody for GFP:SLOMO observation, the bands on the stain-free gel are loading control (e). Quantification of three independent experiments with *slomo-3 pSLOMO::GPF:SLOMO* #31. Letters indicate significant differences based on ordinary one-way ANOVA and Tukey's test ($P < 0.05$) (f). Error bars indicate SE.

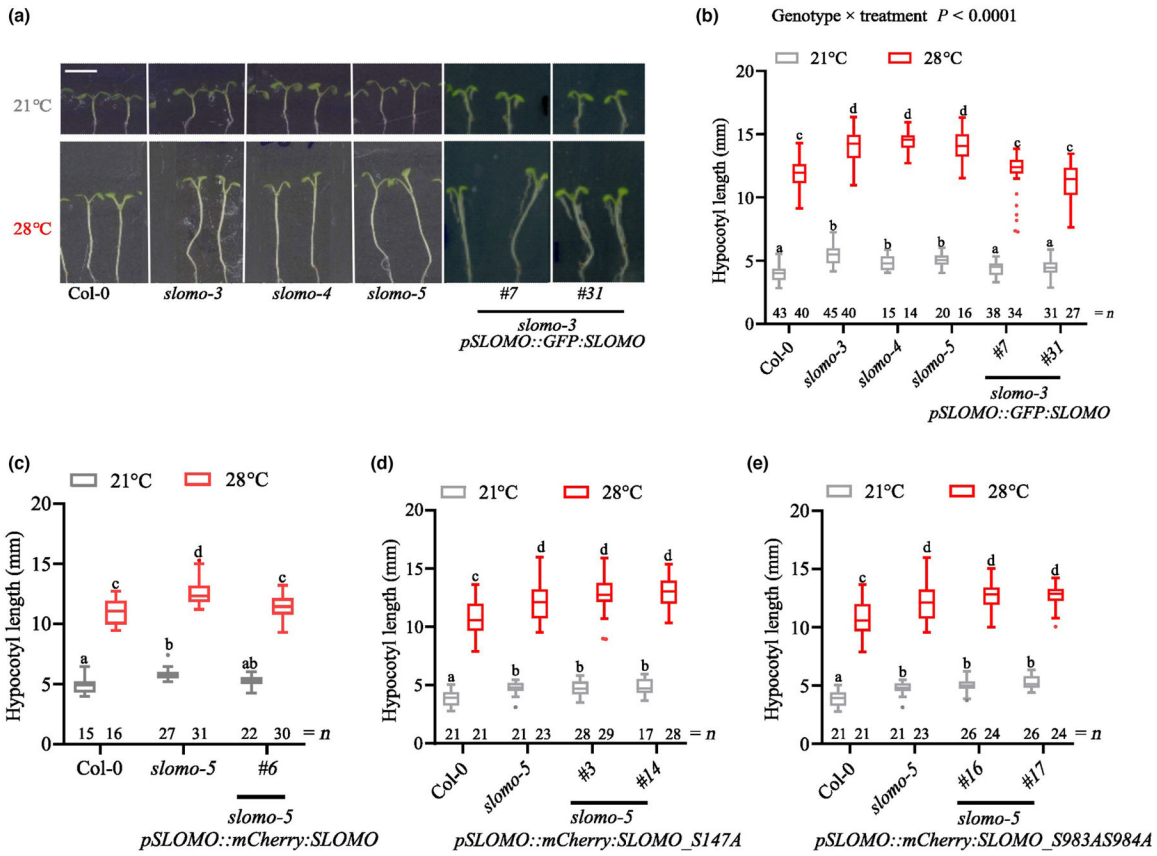

Fig. 4.

SLOMO negatively regulates *Arabidopsis thaliana* hypocotyl growth. (a, b) Representative images (a) and quantification (b) of hypocotyl length of 7-d-old *slomo* mutants and *slomo-3 pSLOMO::GFP:SLOMO* complemented lines compared with Col-0. Bar, 5 mm. Box plots show median with Tukey-based whiskers and outliers. Letters indicate significant differences based on two-way ANOVA and Tukey's test ($P < 0.05$). The number of individually measured seedlings is indicated at the bottom. The experiments were repeated 3 times. The *P*-value for the interaction (genotype × temperature) is shown at the top. (c–e) Quantification of hypocotyl phenotype for indicated lines. Box plots show median with Tukey-based whiskers and outliers. Letters indicate significant differences based on two-way ANOVA and Tukey's test ($P < 0.05$). The number of individually measured seedlings is indicated above the *x*-axis.

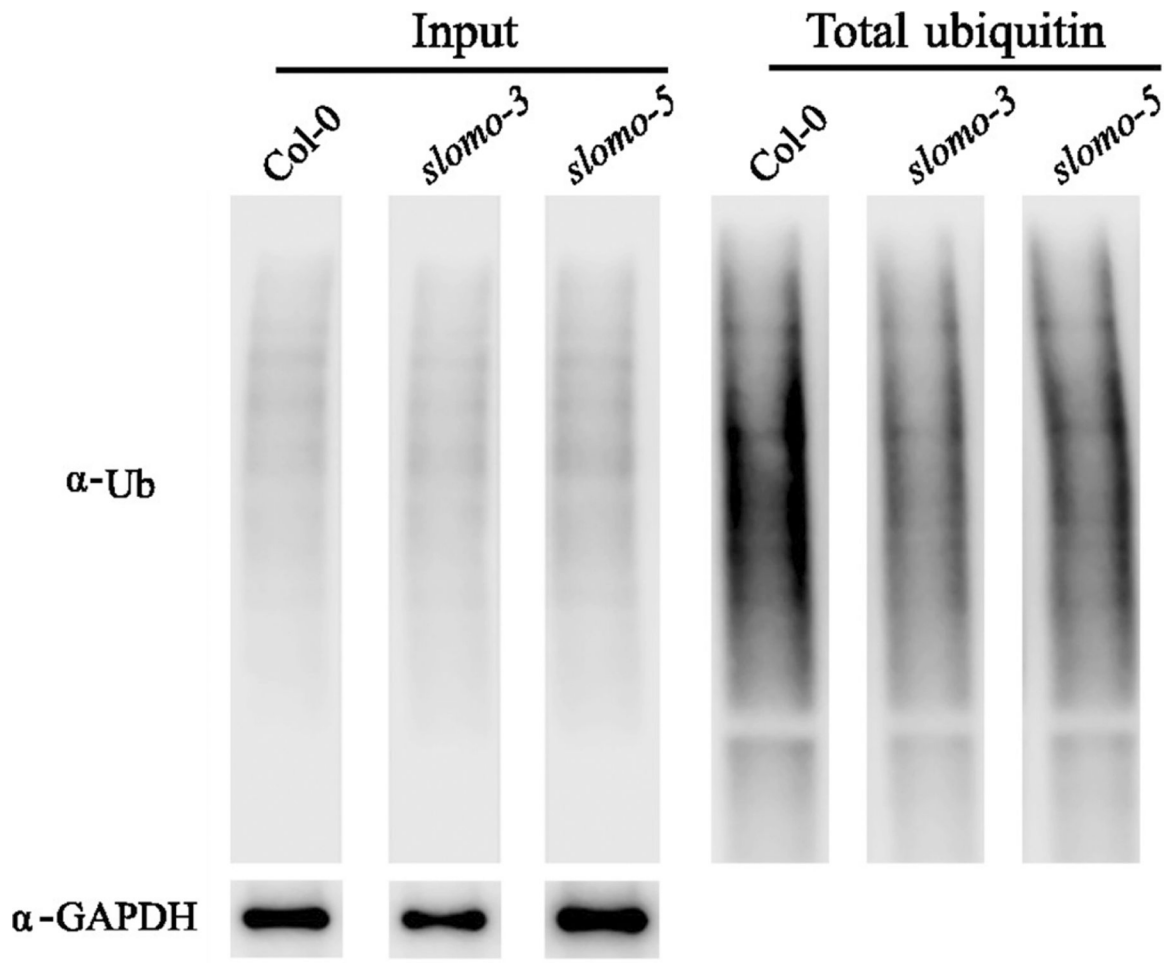

Fig. 5.

Loss of SLOMO function results in reduced ubiquitination in *Arabidopsis thaliana*. Western blot showing total ubiquitin of 9-d-old Col-0 (wild type; WT) and *slomo* mutants at 21°C. Ubiquitinated proteins were pulled down using HALO-ubiquilin. Ubiquitinated protein was detected by anti-ubiquitinylated proteins antibody, clone FK2. GAPDH as the loading control of input was detected by immunoblotting against α-GAPDH antibody.

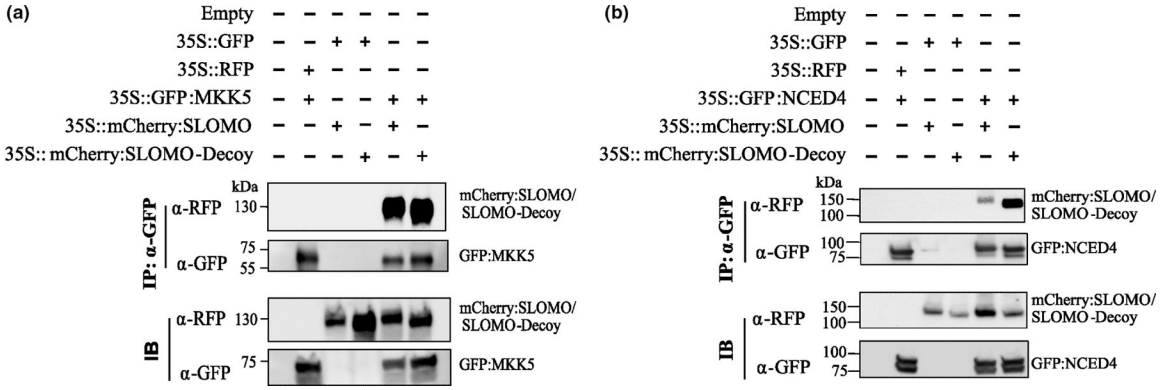

Fig. 6.

Validation of MKK5 and NCED4 interaction with SLOMO. (a, b) Validating the interaction of MKK5-SLOMO and NCED4-SLOMO by Co-IP in *Nicotiana tabacum*, using GFP-trap.

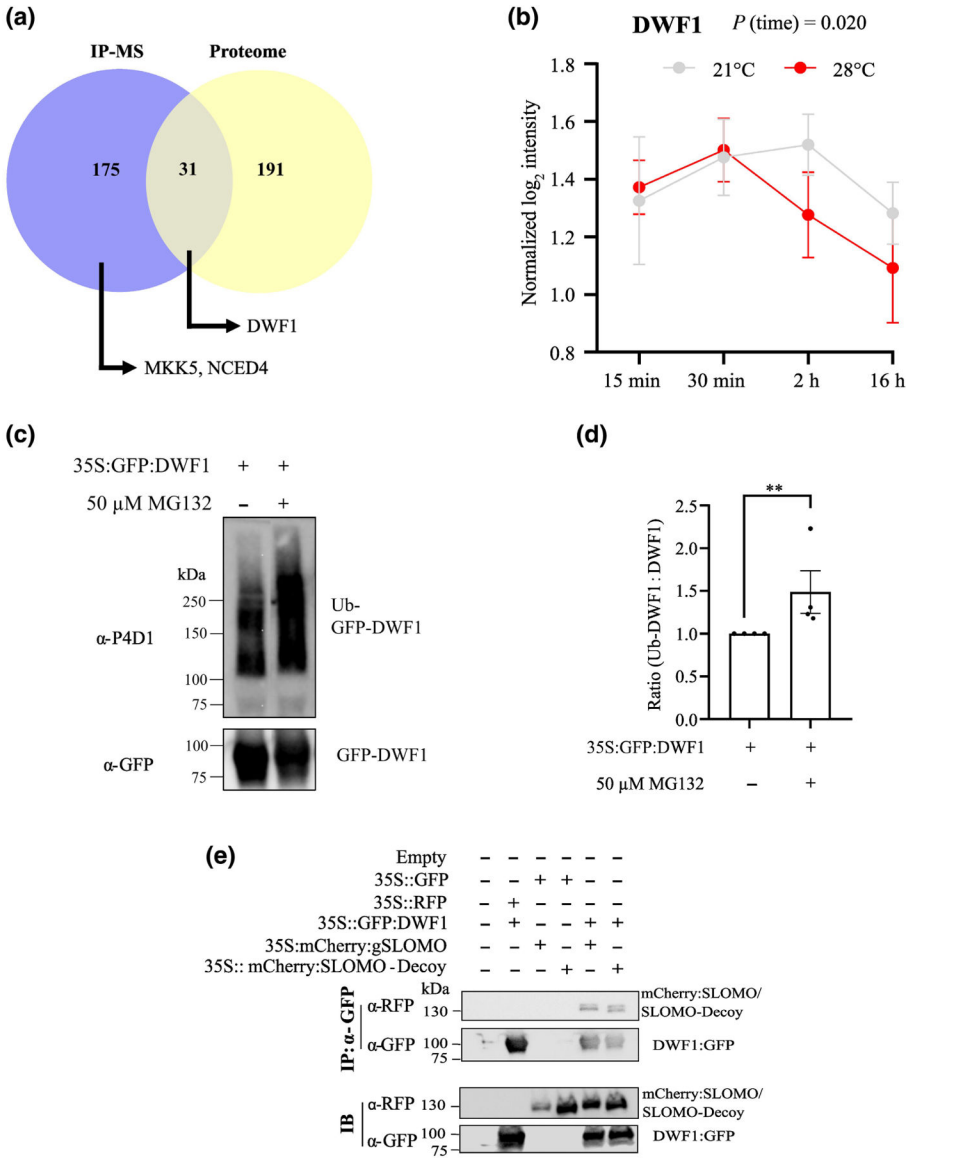

Fig. 7.

DWF1 is likely substrate of SLOMO. (a) Venn diagram of candidates from IP-MS data from 16-d-old *35S::GFP:SLOMO-Decoy* expressing seedlings and from warm temperature-regulated proteome analyses. Relevant candidates are indicated. (b) DWF1 protein abundance in control (21°C) and warm temperature (28°C) time course. (c, d) Western blot (c) and quantification (d) of DWF1 ubiquitination upon expressing *35S:: GFP:DWF1* in *Nicotiana tabacum* treated with or without 50 µM MG132 for 16 h. Ubiquitin was detected after GFP-trap co-IP by α-P4D1, and GFP:DWF1 was detected by α-GFP. The quantification shows the ratio of Ub-DWF1 : DWF1 from four biological replicates (indicated with dots). Asterisk indicates the significance between treatments based on the *t*-test $P < 0.05$. (e) Validation of the interaction between SLOMO and DWF1 by Co-IP in *N. tabacum*. GFP-trap used to do the pull-down. Error bars indicate SE (b, d).

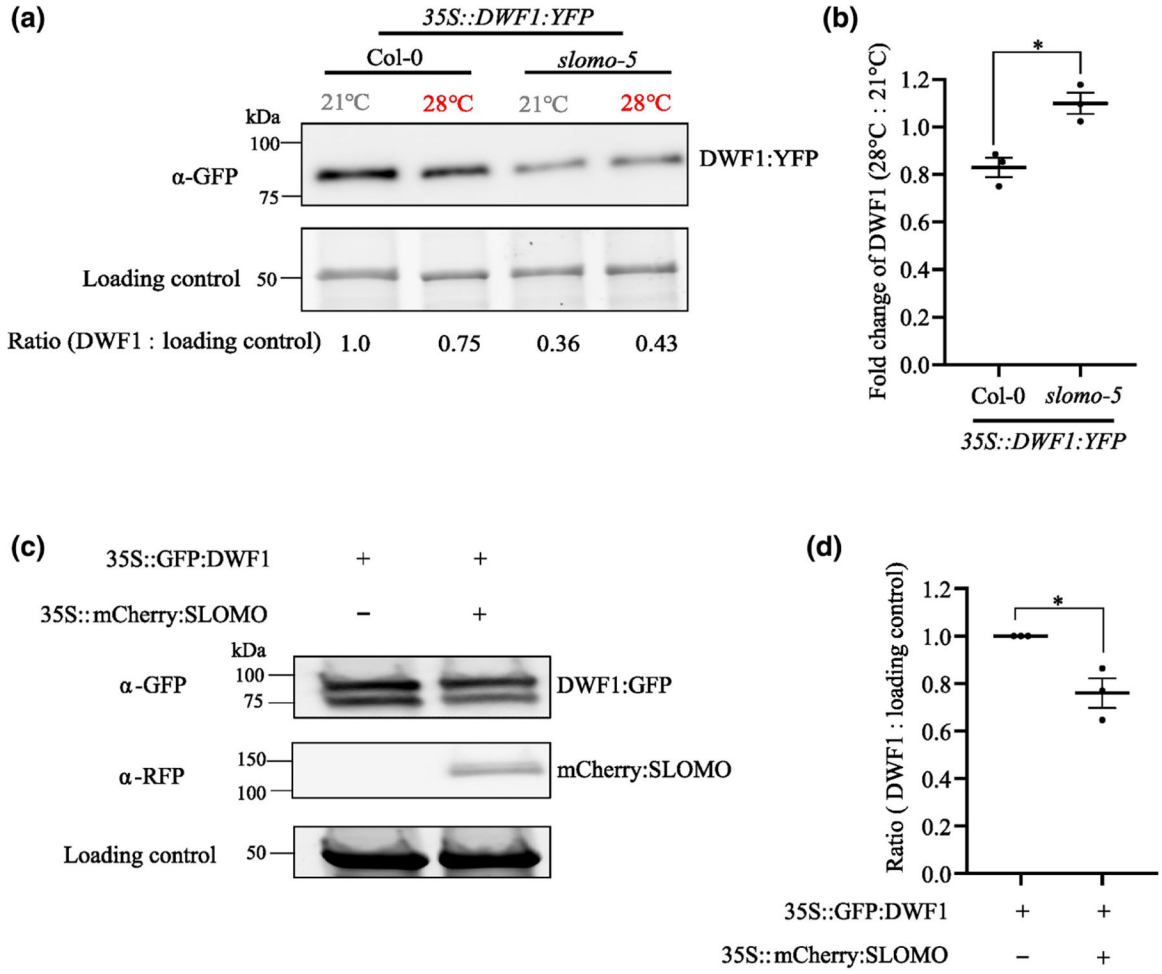

Fig. 8.

SLOMO promotes DWF1 degradation. (a, b) Western blot detecting DWF1 in 7-d-old *35S::DWF1:YFP* and *35S:: DWF1:YFP slomo-5* seedlings transferred to 21°C or 28°C for 2 h. DWF1:YFP was detected with an α-GFP antibody (a). The graph shows fold change of DWF1 (28°C/21°C) (b). (c, d) Western blot detecting DWF1 when expressing *35S::GFP:DWF1* or co-expressing *35S::GFP:DWF1* and *35S:: mCherry:SLOMO* in *Nicotiana tabacum*. The graph shows quantification of relative DWF1 abundance (d). For (a, c), stain-free gel as the loading control. For (b, d), graphs show mean (line) of three biological replicates (individual dots) with SE of the mean. *, Significant differences based on a one-way ANOVA and Tukey's test ($P < 0.05$).

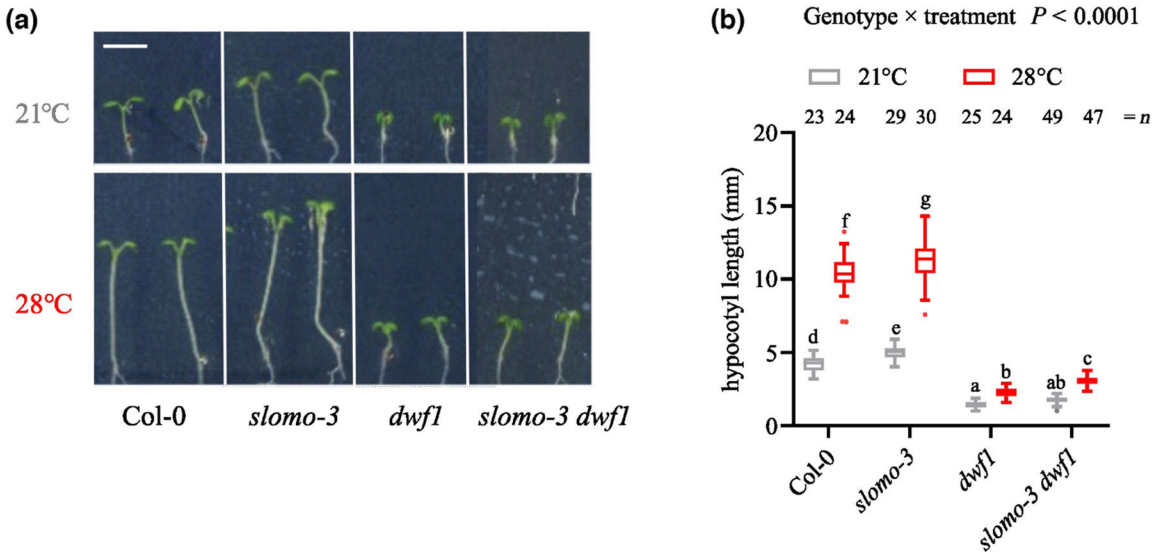

Fig. 9.

Genetic interaction between SLOMO and DWF1 in *Arabidopsis thaliana*. (a, b) Hypocotyl length of 7-d-old *slomo-3* and *dwf1* mutants: representative image. Bar, 5 mm (a) and quantification of hypocotyl length (b). Box plots show median with Tukey-based whiskers and outliers. Letters indicate significant differences based on two-way ANOVA and Tukey's test ($P < 0.05$). The number of individually measured seedlings is indicated at the top. The P-value for the interaction (genotype × temperature) is shown at the top.

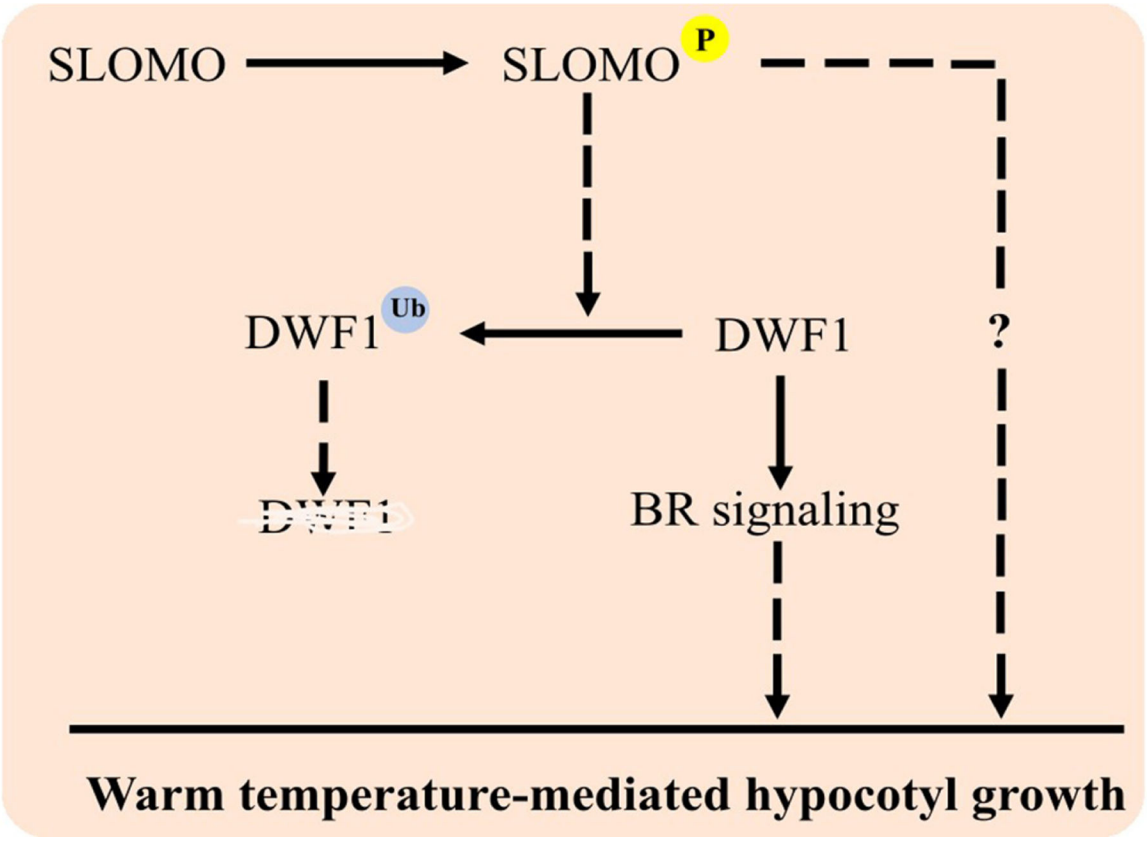

Fig. 10.

Putative model for SLOMO-mediated signaling in (warm temperature-mediated) hypocotyl growth. Warm temperature activates SLOMO activity through phosphorylation (P), which promotes the ubiquitination (Ub) of DWF1, and this affects brassinosteroid (BR) signaling during warm temperature-mediated hypocotyl growth. In parallel, SLOMO also interacts with other unknown substrates (?) to regulate hypocotyl growth upon warm temperature. Light red background indicates warm temperature conditions (28°C). Dashed lines indicate steps that require other known or unknown components that are not indicated here. DWF1 broken up by line indicates degraded DWF1.